Genomic loci mispositioning in *Tmem120a* knockout mice yields latent lipodystrophy

Rafal Czapiewski[1], Dzmitry G. Batrakou[1], Jose I. de las Heras[1], Roderick N. Carter[2], Aishwarya Sivakumar[1], Magdalena Sliwinska[1], Charles R. Dixon[1,3], Shaun Webb[3], Giovanna Lattanzi[4,5], Nicholas M. Morton[2], and Eric C. Schirmer[1,*]

[1]Institute of Cell Biology, University of Edinburgh, Edinburgh, EH9 3BF, UK

[2]Molecular Metabolism Group, BHF Centre for Cardiovascular Science, Queen's Medical Research Institute, University of Edinburgh, Edinburgh, EH16 4TJ, UK

[3]Wellcome Centre for Cell Biology, University of Edinburgh, Edinburgh, EH9 3BF, UK

[4]CNR - National Research Council of Italy, Institute of Molecular Genetics "Luigi Luca Cavalli-Sforza", Unit of Bologna, Bologna, 40136, Italy

[5]IRCCS, Istituto Ortopedico Rizzoli, Bologna, 40136, Italy

Correspondence:

[*]Eric Schirmer, Ph.D.

Institute of Cell Biology

University of Edinburgh, Kings Buildings

Swann 5.22, Mayfield Road

Edinburgh EH9 3BF, UK

Tel:+44(0)1316507075

Fax:+44(0)1316507360

e.schirmer@ed.ac.uk

Running title: TMEM120A loss yields latent lipodystrophy

Author e-mail addresses:

Rafal Czapiewski rafal.czapiewski@ed.ac.uk

Dzmitry G. Batrakou d.batrakou@gmail.com

Jose I. de las Heras J.delasHeras@ed.ac.uk

Roderick N. Carter rod.carter@ed.ac.uk

Aishwarya Sivakumar s1633133@sms.ed.ac.uk

Magdalena Sliwinska madziakorczak7@gmail.com

Charles R. Dixon s1581423@sms.ed.ac.uk

Shaun Webb swebb1@staffmail.ed.ac.uk

Giovanna Lattanzi giovanna.lattanzi@cnr.it

Nicholas M. Morton nik.morton@ed.ac.uk

Eric C. Schirmer e.schirmer@ed.ac.uk

Abstract

Little is known about the proteins that direct the highly conserved patterns of spatial genome organisation in fat. Here we report that adipocyte-specific knockout of the gene encoding nuclear envelope protein Tmem120a disrupts fat genome organisation, thus causing a novel lipodystrophy syndrome. Tmem120a deficiency broadly suppresses lipid metabolism pathway gene expression and induces myogenic gene expression by repositioning genes, enhancers and miRNA-encoding loci between the nuclear periphery and interior. Tmem120a$^{-/-}$ mice, particularly females, exhibit a lipodystrophy syndrome similar to human familial partial lipodystrophy FPLD2, with profound insulin resistance and metabolic defects that manifests upon exposure to an obesogenic diet. Interestingly, similar genome organisation defects occurred in cells from FPLD2 patients that harbour nuclear envelope protein laminA mutations. Our data suggest TMEM120A may mediate/instigate novel categories of adipose tissue dysfunction across the adiposity spectrum and provide a new miRNA-based mechanism possibly driving the unexplained muscle hypertrophy in human lipodystrophy.

Keywords: nuclear envelope transmembrane protein (NET); lipodystrophy; gene positioning; tissue specificity; spatial genome organisation; adipogenesis; muscle repression.

INTRODUCTION

The extremes of adiposity, severe obesity and lipodystrophy, lead to insulin resistance and metabolic disease. These disorders often arise from rare protein-coding mutations causing adipose tissue dysfunction; however, genome association studies also point to more complex mechanisms[1,2,3]. For example mutations in remote enhancers that disrupt adipocyte-specific gene expression are now linked to adiposity pathologies[1,2,3] and alterations in genome organisation that block enhancer-gene interactions are demonstrated to disrupt tissue development leading to disease[4,5]. Previous studies have yet to identify proteins controlling adipocyte-specific genome organisation, though such organisation is a critical hierarchical determinant of tissue differentiation and gene expression through directing genes to active/inactive regions and enabling enhancer-gene contacts.

The nuclear envelope (NE) actively directs radial genome organisation, releasing for activation genes needed for tissue differentiation and function while recruiting for repression genes antagonistic to tissue function[6]. Importantly, radial genome organisation is disrupted in diseases linked to NE proteins such as laminA, mutations in which cause familial partial lipodystrophy of the Dunnigan-type (FPLD2)[7,8], a more severe lipodystrophy[9], several metabolic syndromes[10,11], and type 2 diabetes[12,13]. The relevance of genome organisation for adiposity was first indicated by findings that critical pro-adipogenic genes *FABP4*, *PPARG*, *CREB* and *CEBPB* reposition from the NE to nuclear interior in adipogenesis[14]. LaminA was the first NE protein linked to adipogenesis, with >1,000 genes under NE/laminA positional regulation in adipocytes[15,16]. However, laminA is widely expressed while several tissue-specific NE transmembrane proteins (NETs) direct specific gene repositioning during development of the tissues where they are expressed[17,18,19]. Of these, TMEM120A (called NET29) is highly expressed in both white adipose tissue (WAT) and brown adipose tissue (BAT). Brain is one of the few other tissues expressing *Tmem120a*

mRNA and antibodies detected a larger mass Tmem120a protein in mouse brain, suggesting a different splice variant is expressed in the nervous system[20].

Tmem120a gene knockdown in mouse 3T3-L1 preadipocytes reduced adipogenesis and lipid accumulation ~30% and combined knockdown with its paralog *Tmem120b* reduced it ~60%[20]. Notably, TMEM120A re-expression in double knockdown 3T3-L1 cells elicited superior adipogenic rescue than TMEM120B, suggesting a dominant role of TMEM120A in adipogenesis. In humans, *TMEM120A* was downregulated in adipose tissue of obese Arizona Pima Native Americans[21] and in obesity with diabetes (data obtained from GEO dataset, GDS3665), with both studies showing stronger effects in females. *Tmem120a* is also upregulated by cold-exposure in WAT of mice[22] and by treatment of cells with rosiglitazone, an agonist of the master adipogenic transcription factor PPARγ, that improves insulin sensitivity in diabetes[23]. Interestingly, *Tmem120A* was one of the genes with most altered expression in hypothalamus of chickens genetically selected for fat accumulation[24]. Perhaps relevant to this, TMEM120A (called TACAN) was recently hypothesized to be involved in nociception in brain[25].

Here we investigated the impact of adipocyte-specific *Tmem120a* gene disruption on genome organisation and fat metabolism in mice *in vivo*. We find that loss of Tmem120a leads to a distinct but latent lipodystrophy pathology, similar to FPLD2, that we show is due to a novel disease pathomechanism: loss of Tmem120a alters positioning of multiple genes, enhancers, and miRNA-encoding loci resulting in multiple gene expression defects. This is the first demonstration of miRNA-encoding loci under NE positional regulation and it suggests that lipodystrophy-associated skeletal muscle hypertrophy could be paracrine mediated.

RESULTS

Adipocyte–specific *Tmem120a*$^{-/-}$ Mice Exhibit Reduced White Adipose but Increased Brown Adipose Fat Accumulation on a High Fat Diet

Given that *Tmem120a* knockdown in 3T3-L1 *in vitro* adipogenesis reduced expression of several genes central to adipocyte metabolism[20], we sought to determine effects of Tmem120a loss on adiposity and metabolism in mice. Mating a conditional knockout line with exons 2 and 3 floxed (*Tmem120a*$^{fl/fl}$) to Adiponectin-Cre (Adip$^{Cre/+}$) mice[26,27,28] generated an adipocyte–specific knockout (*Ad-Tmem120a*$^{-/-}$; Supplementary Fig. 1a-d). Littermates, homozygotes *Tmem120a*$^{fl/fl}$ without the Adip-Cre allele were used as a control for all experiments. Adip$^{Cre/+}$ deletor mice were used because it is more specific for adipose tissue than the alternate Ap2^{Cre} mice that express Cre in brain[28,29], which was important since a larger Tmem120a variant is expressed in brain. Accordingly, we confirmed that Tmem120a was still expressed in brain of the *Ad-Tmem120a*$^{-/-}$ mice (Supplementary Fig. 1d). We anticipate that early differentiation functions of Tmem120a will still occur since it is expressed 2-4 days earlier than adiponectin[20]; so our use of Adip$^{Cre/+}$ should preferentially highlight Tmem120a metabolic functions in mature adipocytes.

Mice on standard diet (13.5% fat, 43% carbohydrates, 29% protein) showed sex specific differences in body weight. By 20 weeks of age female *Ad-Tmem120a*$^{-/-}$ animals began to weigh significantly less than controls (Supplementary Fig. 1e). Interestingly, a difference in male body weight, although modest, was observed only between weaning and young adulthood (weeks 4-8; Supplementary Fig. 1f). To test if the body weight differences were exaggerated by different caloric loads, mice raised initially on a standard diet were switched to either a low-fat diet (LFD; 10.5% fat, 73.1% corn starch, 16.4% protein) or a high-fat diet (HFD; 58% fat, 25.5% sucrose, 16.4% protein) at 12 weeks of age. Body weight was measured weekly, revealing greatly reduced weight gain specifically on HFD–fed female *Ad-Tmem120a*$^{-/-}$ mice compared to littermate controls (Fig. 1a,b). At 9-10 weeks post-HFD, a peak difference of ~25%

total body weight was observed that corresponded to >50% less weight gained in the knockout. There was no difference in food intake on HFD between genotypes (Fig. 1c) suggesting altered energy expenditure most likely accounts for the difference in the gain of body weight. Body weight effects of altered caloric loads were also sex-specific with no difference between male *Ad-Tmem120a*$^{-/-}$ mice and control littermates on either LFD or HFD (Supplementary Fig. 1g).

TD-NMR body composition analysis showed that weight differences were driven by a >40% reduction in gained fat mass using normalised data for *Ad-Tmem120a*$^{-/-}$ females compared to control littermates (Fig. 1d) that was even stronger using non-normalised data (Supplementary Fig. 1k). This difference was partially offset by an increase in lean mass, limiting the difference in total body weight gained to ~25% (Fig. 1e, normalised; Supplementary Fig. 1l, non-normalised). *Ad-Tmem120a* loss had no effect on males (Supplementary Fig. 1h,l). Reduced fat accumulation in females was also depot dependent. After normalising isolated depot weight to total body weight, gonadal WAT exhibited the largest difference in gained fat mass (>40%) followed by subcutaneous inguinal WAT (iWAT; ~20%) (Fig. 1f).

To test if relative lack of fat mass accumulation in *Ad-Tmem120a*$^{-/-}$ females on HFD was accounted by reduced cell numbers (hyperplasia) or reduced fat accumulation (hypertrophy), we visually investigated fat stores and quantified cell sizes. iWAT had similar morphology and appearance for droplet/adipocyte numbers per field between *Ad-Tmem120a*$^{-/-}$ and control littermates on LFD indicating no loss in generation of fat cells during differentiation (Fig. 1g). However, on HFD the size of fat droplets in iWAT cells visibly increased in control littermates compared to *Ad-Tmem120a*$^{-/-}$ mice (Fig. 1g). Interestingly, this situation was inverted for BAT where fat droplet size per cell greatly increased in *Ad-Tmem120a*$^{-/-}$ mice compared to control littermates on HFD (Fig. 1h). Quantification revealed ~2.5-fold increase for iWAT lipid droplets >10,000 μm^2 in size specifically for control littermates on HFD (Fig. 1i,j) whereas a ~3-fold increase in lipid droplets >200 μm^2 occurred in BAT from *Ad-*

Tmem120a$^{-/-}$ mice on HFD (Fig. 1k,l). Individual organs showed no difference in weight normalised to body weight except a small increase in brain and small shortening of body (~1 cm) and tail (~0.5 cm) length (Supplementary Fig. 1m,n) in *Ad-Tmem120a*$^{-/-}$ mice on HFD, again specific to females.

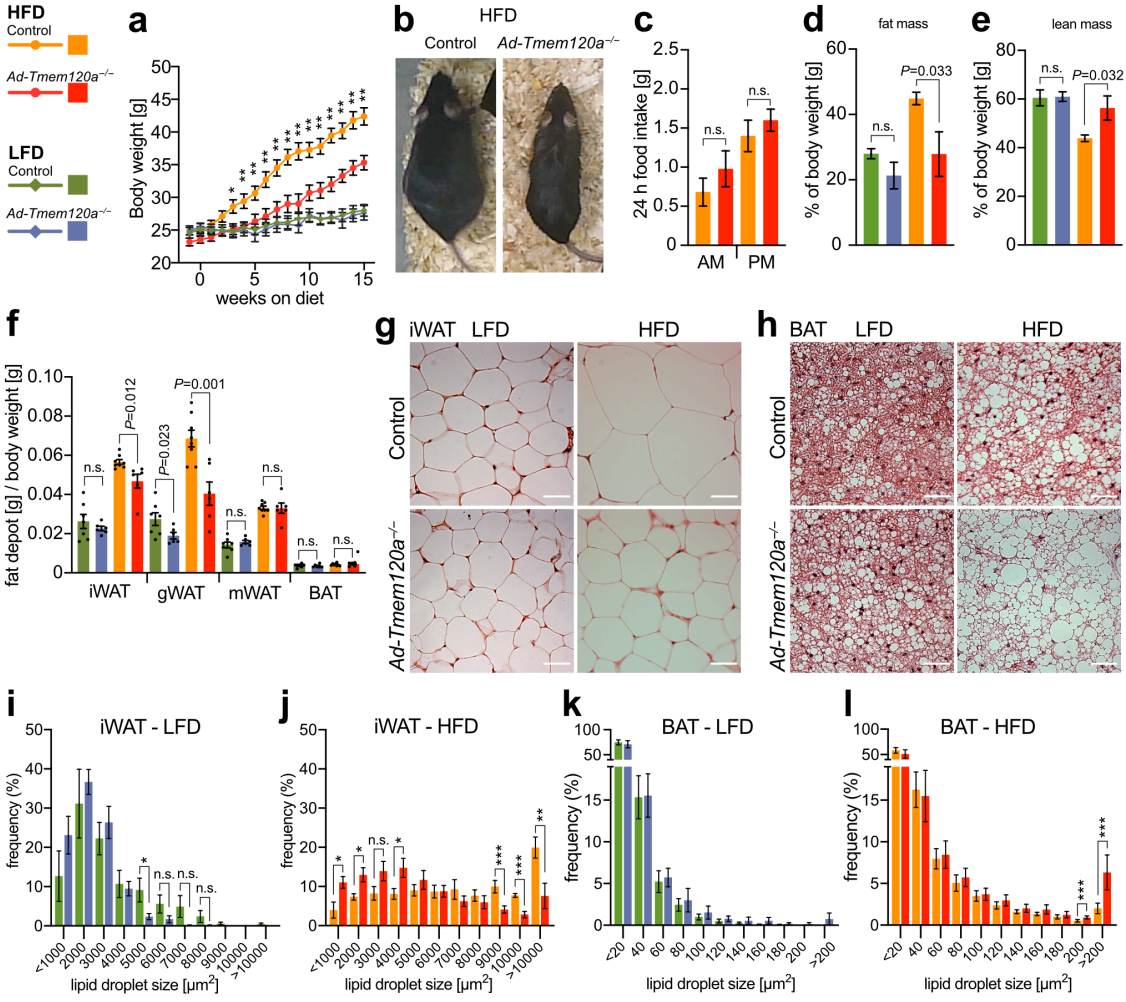

Fig. 1. *Ad-Tmem120a*$^{-/-}$ Mice Have Reduced Fat Accumulation in WAT While Fat Is Increased in BAT

a, Female body weight on high-fat (HFD) vs low-fat (LFD) diet. Data from two separate experiments, shown as mean SEM (n=9-10 per group), **P* <0.05, ***P*<0.01 by unpaired Student's *t*-test. **b**, Representative images of 6-month-old female mice, control and *Ad-Tmem120a*$^{-/-}$ mice after 10 weeks on HFD. **c**, 24 h food intake by females on HFD [g]; shown as mean SEM (n=4), n.s. – not statistically significant. **d** and **e**, Female mice body composition measured by TD-NMR after 10 weeks of LFD and HFD, fat mass (**d**) and lean mass (**e**) are shown as percent of whole-body weight; shown as mean SEM (n=4). **f**, Whole body mass-normalised weight of different adipose tissue depots: inguinal-subcutaneous (iWAT), gonadal (gWAT), mesenteric (mWAT) and interscapular BAT, shown as mean SEM (n=6-8). **g** and **h**, Images of haematoxylin and eosin stained iWAT (**g**) and interscapular BAT (**h**), from control and *Ad-Tmem120a*$^{-/-}$ female mice on HFD vs LFD, scale bars 40 µm. **i-l**, Quantification of lipid droplet size in iWAT and BAT form control and *Ad-Tmem120a*$^{-/-}$ females on LFD and HFD, the sizes of the lipid droplets were assigned to size bins and are shown as frequency, area in µm^2, shown as mean SEM (n=6-7), **P* <0.05, ***P*<0.01, ****P*<0.001 by unpaired Student's *t*-test. See also Supplementary Fig. 1.

Obesity-resistance in *Ad-Tmem120a*$^{-/-}$ Mice Is Associated with Insulin Resistance

To determine the impact of adipose *Tmem120a* deletion on metabolic homeostasis we performed glucose (GTT) and insulin tolerance tests (ITT). *Ad-Tmem120a*$^{-/-}$ mice showed a mild impairment of glucose tolerance on LFD compared to control littermates that became pronounced on HFD (Fig. 2a,b), suggestive of insulin resistance. We confirmed this with ITT, where *Ad-Tmem120a*$^{-/-}$ mice showed relatively impaired glucose suppression response to insulin compared to control littermates on HFD (Fig. 2c). Consistent with prevailing insulin resistance after HFD exposure, fasting serum insulin levels for these mice were markedly higher for *Ad-Tmem120a*$^{-/-}$ than control littermates (Fig. 2d).

Further consistent with constrained adipose expansion and adipose–derived insulin resistance, serum leptin (Fig. 2e) and adiponectin (Fig. 2f) levels were reduced in *Ad-Tmem120a*$^{-/-}$ mice on HFD compared to control littermates. Hyperlipidemia has been reported in 42% of all lipodystrophy patients, most lamin-linked FPLD2 patients, and some of the wide spectrum of other lamin-linked lipodystrophies and metabolic syndromes[30,31,32]; however, fasting triglyceride and free fatty acid levels were comparable between genotypes on both diets (Fig. 2g,h and Supplementary Table 1). One possible explanation for the lack of elevated serum triglycerides would be if lipids accumulate in liver; however, there was no difference in liver weight between wild-type and knockout (Supplementary Fig. 1m). Liver fat droplet size was also no different (Fig. 2i) and there were no visual indications of hepatic steatosis (Fig. 2j). Notably, *Ad-Tmem120a*$^{-/-}$ mice displayed polydipsia, indicative of worsened diabetes on the HFD, compared to littermates (Fig. 2k).

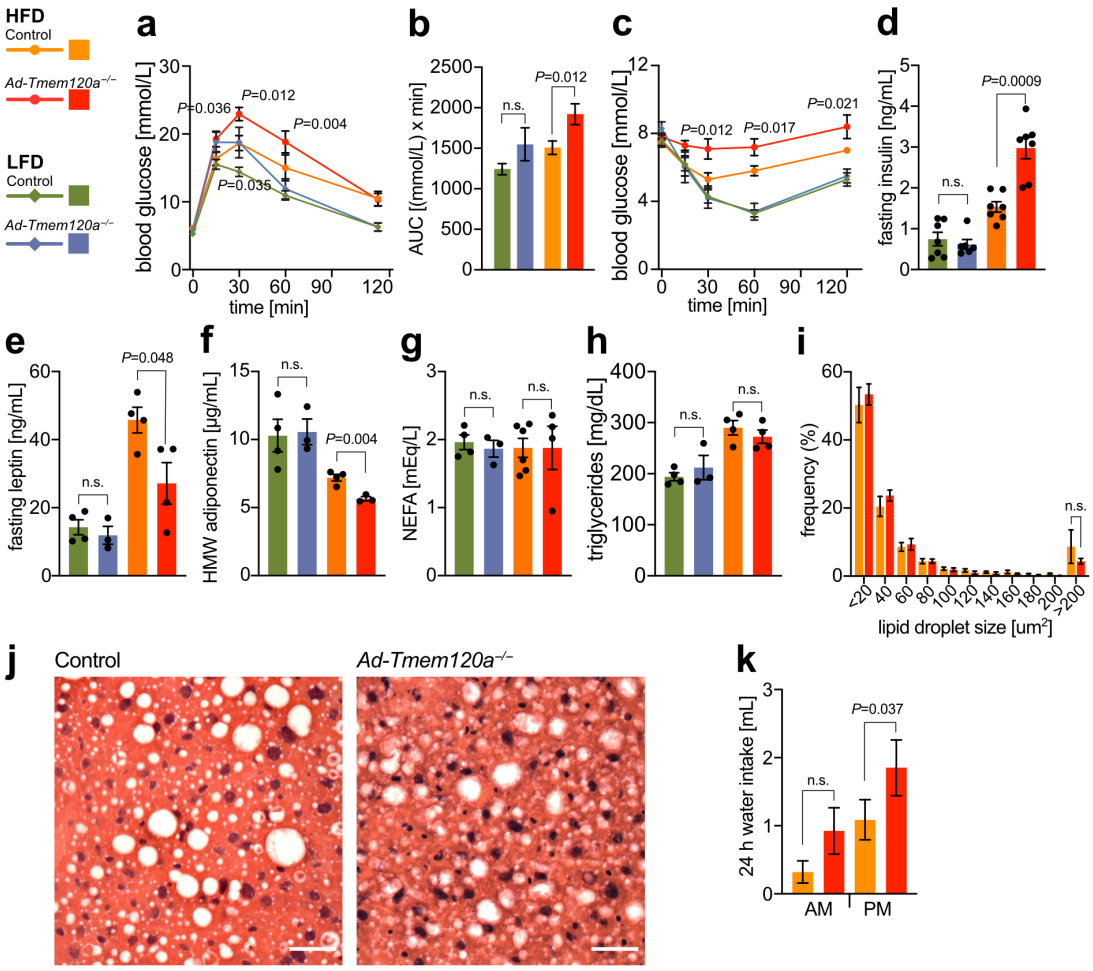

Fig. 2. Insulin resistance in *Ad-Tmem120a*$^{-/-}$ Mice

a and **b**, Glucose tolerance test in control and *Ad-Tmem120a*$^{-/-}$ females on LFD vs HFD, fasting for 16h (**a**), and quantification of the area under the curve (AUC) (**b**), both panels shown as mean SEM, (n=8-10 per genotype and diet). **c**, Insulin tolerance test in control and *Ad-Tmem120a*$^{-/-}$ females on LFD vs HFD, fasting for 6h, shown as mean SEM, (n=5-8). **d-h**, Blood biochemistry. Fasting serum insulin (**d**), fasting leptin (**e**), high molecular weight (HMW) adiponectin (**f**), NEFA - nonestrified fatty acids (**g**), and triglycerides levels (**h**) in control and *Ad-Tmem120a*$^{-/-}$ females on LFD vs HFD, fasting for 16h, shown as mean SEM, (n=3-7). **i**, Quantification of lipid droplet size in liver form control and *Ad-Tmem120a-/-* females on HFD, the sizes of the lipid droplets were assigned to size bins and are shown as frequency, area in µm2, shown as mean SEM (n=3). n.s. - not statistically significant, by unpaired Student's t-test. **j**, Representative images of haematoxylin and eosin-stained liver sections from control and *Ad-Tmem120a-/-* female mice on HFD, scale bars: 40 µm. **k**. Mean daily water intake by control and *Ad-Tmem120a*$^{-/-}$ females after 10 weeks on HFD, shown as mean SEM, (n=4), *P* values: by unpaired Student's *t*-test.

Ad-Tmem120a$^{-/-}$ Mice Retain Partial Carbohydrate Utilization on HFD

To determine whether altered substrate utilisation underpinned the constrained fat accumulation in *Ad-Tmem120a*$^{-/-}$ female mice, we performed indirect calorimetry analysis. There were no differences between genotypes on standard diet or after initial exposure to HFD (Fig. 3a-d), but by 8 weeks of HFD divergence in metabolic

responses was strong. Control littermate mice on HFD exhibited the expected suppression of diurnal cycling between fat and carbohydrate utilisation, with a consistent lipid burning respiratory exchange ratio (RER) approaching 0.7 (Fig. 3e). In contrast, *Ad-Tmem120a*$^{-/-}$ mice maintained a consistently higher RER than littermate controls, indicative of partially retained carbohydrate utilisation across day and night periods (Fig. 3e). Energy expenditure differed significantly between the genotypes (Fig. 3f) despite comparable physical activity (Supplementary Fig. 3a-f).

To assess metabolic activity at the cellular level, we generated adipocytes using isolated primary stromal vascular cells from subcutaneous adipose depots of *Tmem120a*$^{fl/fl}$ mice. Knockout was achieved *in vitro* by infection with AAV carrying Cre upon induction of adipogenesis. Notably, knockout cells had smaller lipid droplets upon differentiation compared to the same cells infected with AAV virus carrying GFP only (Supplementary Fig. 3g-i). The differentiated cells were analysed for bioenergetics using a Seahorse flux analyser. *Tmem120a* knockout cells had higher basal and maximal respiration (Fig. 3g,h and Supplementary Fig. 3j) that was driven by higher proton leak as ATP-linked respiration was comparable to the control. To address the dependency on carbohydrate fuel utilisation, we repeated this analysis with UK5099 to inhibit mitochondrial pyruvate uptake (Fig. 3i,j). Consistent with animals increased carbohydrate utilisation, the knockout adipocytes were more dependent on mitochondrial pyruvate to support respiration. Therefore, whole animal and cellular data both indicate Tmem120a is important in adipocyte fuel substrate utilisation.

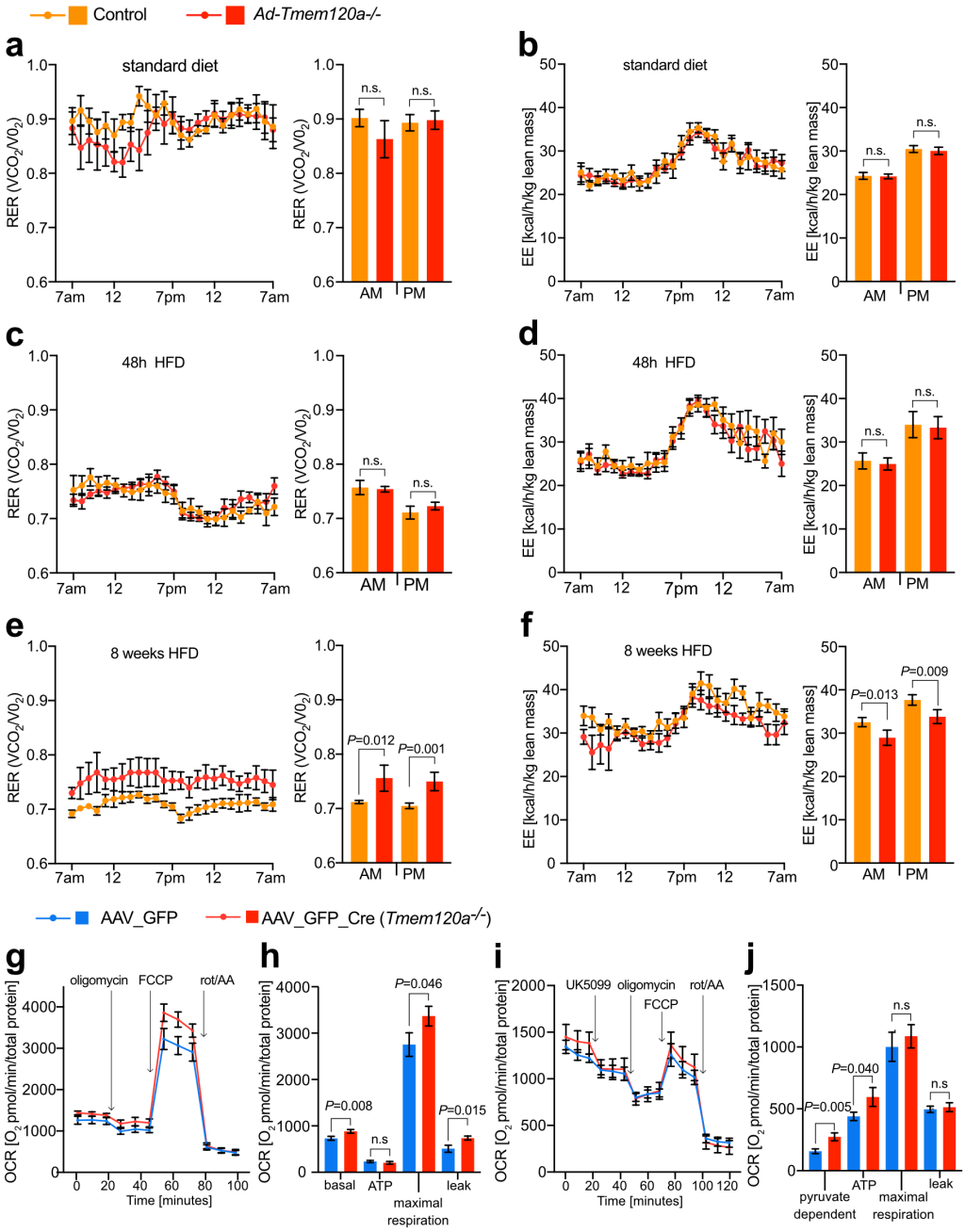

Fig. 3. Oxidative Metabolism Is Altered in *Ad-Tmem120a*$^{-/-}$ Mice

a and **b**, Indirect calorimetry on standard diet female control and *Ad-Tmem120a*$^{-/-}$ mice, respiratory exchange rates – RER (VCO_2/VO_2) (**a**), and energy expenditure – EE [kcal/h/kg lean mass] (**b**). Line graphs show representative 24h trace means SEM and bar graphs show 48h means SEM, (n=4), *P* values: by unpaired Student's t test. **c** and **d**, RER trace (**c**) and EE (**d**) in control and *Ad-Tmem120a*$^{-/-}$ female mice treated with high fat-diet for 48h. **e** and **f**, RER trace (**e**) and EE (**f**) in control and *Ad-Tmem120a*$^{-/-}$ female mice treated with high fat-diet for 8 weeks. **g** and **h**, Oxygen consumption rates (OCR) in stromal vascular fraction cells (SVF) differentiated into adipocytes isolated from lox/lox animals infected with AAV_GFP_Cre to obtain *Tmem120a* knockout and control AAV_GFP. Mitochondria stress experiment in the presence of oligomycin, an ATPase inhibitor, FCCP – mitochondrial respiration uncoupler (maximal respiration) and rotenone with antimycin A (rot/AA) – electron transport chain complex I and III blockers, respectively. OCR traces normalised to total protein are shown as means SEM (**g**) and non-mitochondrial respiration-normalised quantification of OCR is shown on a bar chart graph (**h**) as means SEM, (n=4). *P* values: by unpaired Student's *t*-test. **i** and **j**, Pyruvate dependency in SVF adipocytes from lox/lox mice subcutaneous fat infected with AAV_GFP or AAV_GFP_Cre as OCR was measured upon delivery of UK5099. See also Supplementary Fig. 3.

Adipogenic Genes Are Repressed and Myogenic Genes De-repressed in Inguinal Fat from *Ad-Tmem120a*$^{-/-}$ Mice

As TMEM120A functions in genome organisation/ expression regulation[19,33], we considered that the multiple effects on adipocyte metabolism and function might reflect multiple genes affected by TMEM120A loss. Indeed, RNA-Seq on inguinal subcutaneous WAT stores revealed 116 genes altered in expression in *Ad-Tmem120a*$^{-/-}$ mice compared to control littermates (Fig. 4a and Supplementary Table 2). To determine if these genes had adipocyte functions that could potentially explain the metabolic defects in the mouse, we extracted their Gene Ontology (GO) terms and separately plotted the fraction of down- or up-regulated genes with a particular (GO) Biological Process. Strikingly, the GO-terms most commonly associated with downregulated genes strongly related to metabolism: out of the total downregulated genes in the knockout >40% had metabolism functions (Fig. 4b). Focusing on GO-terms associated with the most downregulated genes revealed that gene functions reduced more than 10-fold included gluconeogenesis and aromatic amino acid metabolism. Individual gene product links to adipocyte function and metabolism ranged from formyl peptide receptor 1 (*Nfpr1*) that interacts with gut-microbiota generated N-formyl peptide to promote obesity-linked glucose intolerance[34] to protein tyrosine phosphatase receptor type V (*Ptprv*) that regulates insulin secretion[35] to Nos1ap that increases oxidative stress in diabetes[36] and contributes to adipose tissue beiging[37]. Thus, distinct functions of different genes altered in the knockout could explain different aspects of the lipodystrophy pathology and comorbidities.

The genes most strongly upregulated encoded pro-myogenic proteins or factors that suppress adipogenesis. Plotting the fraction of upregulated genes with a particular GO Biological Process out of the total upregulated genes in the knockout revealed nearly all the top functions relating to muscle (Fig. 4c). Strikingly, most upregulated genes normally are preferentially expressed in muscle (Fig. 4d): thus, it seems Tmem120a strengthens adiposity in part by enhancing repression of genes

from this related tissue. This parallels previous findings of a muscle specific NET that represses adipose genes in muscle[18].

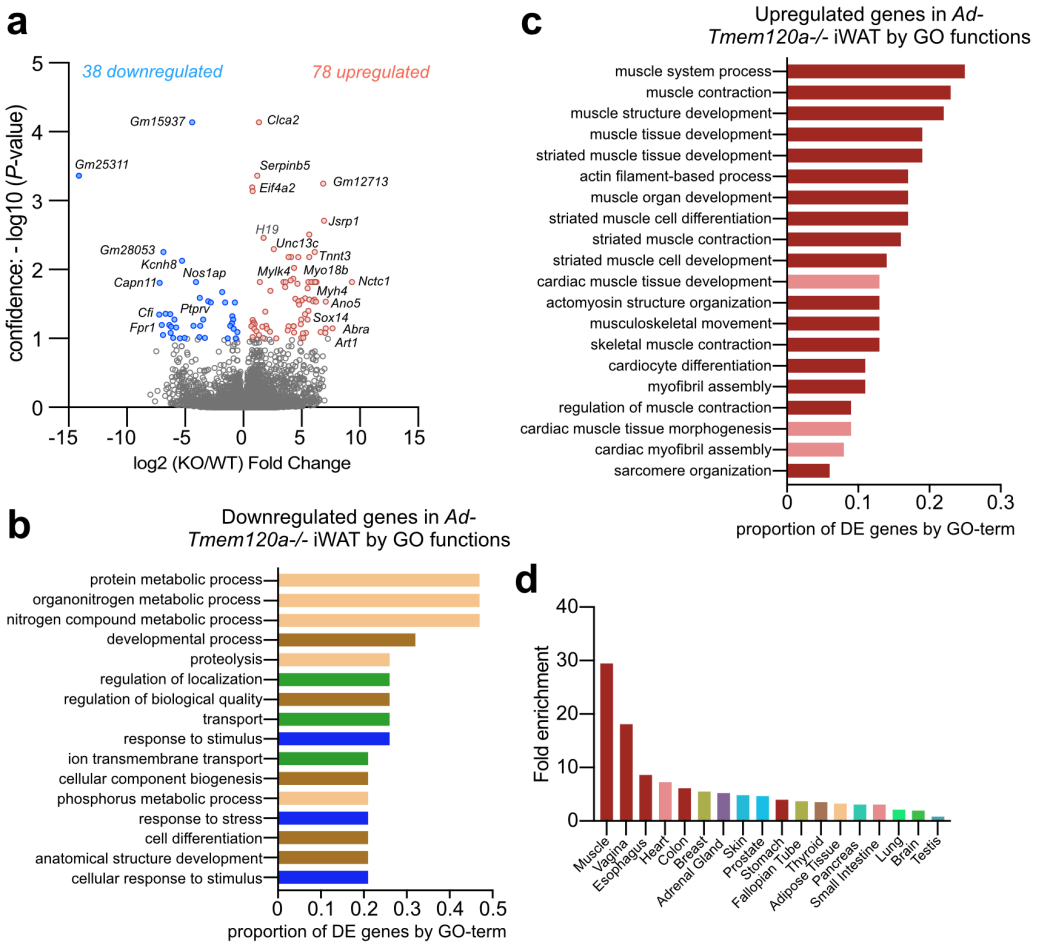

Fig. 4. *Ad-Tmem120a*$^{-/-}$ Mouse Exhibits De-Repression in Inguinal WAT of Many Genes That Normally Repress Myogenesis

a, Volcano plot of genes altered in inguinal subcutaneous white adipose tissue from control and *Ad-Tmem120a*$^{-/-}$ female mice on HFD (n=5). **b**, Gene Ontology (GO) Biological Process analysis for downregulated genes. GO terms found to be significantly enriched using g:Profiler fall into four classes: metabolism (beige), development (brown), transport (green) and response to stimulus (blue). The bars represent the proportion of genes associated with each individual enriched GO term that are present in the downregulated genes dataset. **c**, Gene ontology (GO) Biological Process of analysis for upregulated genes. All of the enriched GO terms are related to muscle function, either skeletal (dark red) or cardiac (pale red). The bars represent the proportion of genes associated with each individual enriched GO term that are present in the upregulated genes dataset. **d**, Tissue-specific gene enrichment for upregulated genes in iWAT from *Ad-Tmem120a*$^{-/-}$ mouse by TissueEnrich tool presented as fold enrichment.

Tmem120a Repositions Genes Between the Nuclear Interior and the NE During 3T3-L1 Adipogenesis

To globally determine genome regions changing between the NE and interior during adipogenesis and the subset of these under Tmem120a regulation we used

DamID that fuses bacterial dam methylase to laminB1 to confer unique methylation to NE-associated DNA so it can be enriched and identified[38,39]. As this approach was not amenable to primary adipocytes we used the well characterized 3T3-L1 *in vitro* adipogenesis system[40,41] that has the advantages of robust transfectability and differentiation and a wealth of literature to relate positioning data to other genomic datasets. Moreover, it allowed us to test for functional redundancy between Tmem120a and its paralog Tmem120b. LaminB1-DamID profiles were obtained for control 3T3-L1 pre-adipocytes and differentiated adipocytes with or without *Tmem120a* knockdown or *Tmem120a*/*Tmem120b* knockdown. As Tmem120a is barely detectable in 3T3-L1 pre-adipocytes and strongly induced upon induction of differentiation, no detrimental effects of expressing knockdown shRNAs prior to differentiation were expected. *Tmem120a* knockdown was >90% compared to an integrated empty shRNA vector control in differentiated cells as previously described[20]. Cells were transduced with laminB1-Dam methylase lentivirus either undifferentiated or at 6 days after pharmacological induction of adipogenesis.

Genomic DNA was isolated from pre-adipocytes after 2 days to ensure cells did not reach confluency (that partly induces differentiation) or from 3-day transduced adipocytes (day 9 of differentiation), enriched for Dam methylated DNA, sequenced, and Log2(LaminB1 Dam/soluble Dam) ratios were generated to identify lamina associated domains (LADs). There was little difference in the total percentage of the genome in LADs, being between 43.7% and 45.1% in all conditions (Fig. 5a; Supplementary Table 3). Similar to DamID in other differentiation systems[18,42,43], the vast majority (~90%) of pre-adipocyte LADs were retained in adipocytes: for those changing, referred to as Differential Regions (DRs), 3.9% of the genome was in LADs that were lost and 4.1% in LADs that were gained during adipocyte differentiation (Fig. 5a and Supplementary Table 3). Similar to a study on muscle NETs in myogenesis[18], DRs tended to be at the edges of pre-existing LADs that either truncated (87%) or became expanded (53%) upon differentiation.

Of the genes located within adipogenesis DRs, 577 were in newly formed LADs and 1,104 in lost LADs. Roughly a third of those released (385; 35%) were under Tmem120a positional regulation, failing to be released when *Tmem120a* was knocked down. The numbers increased to 43% (480 genes) when considering those that failed to be released in the *Tmem120a*/*Tmem120b* double knockdown. For those in newly formed adipocyte LADs, 24% (136) were under Tmem120a positional regulation and 28% (161) were under combined Tmem120a/Tmem120b positional regulation. To directly match repositioning and expression changes, we used microarrays on RNA isolated from parallel samples to the DamID. GO analysis for these revealed similar functions as the genes changing expression in iWAT from the *Tmem120a*$^{-/-}$ mice (Supplementary Fig. 5a,b). Intersecting the set of genes changing position and those changing expression during differentiation revealed that ~10% of genes that changed position also changed expression, also consistent with previous studies. Of the 1,104 genes in lost LADs, 94 increased expression while, of the 577 genes recruited to newly formed LADs, 56 reduced expression (Fig. 5b,c Supplementary Table 3). A subset of these were under Tmem120A positional regulation (highlighted in yellow), but they tended to be relevant to fat metabolism and lipodystrophy associated comorbidities. For example, genes at DRs normally moving to the NE to become repressed that failed to move and failed to be repressed in the Tmem120a knockdown included *Cpe* that yields obesity in mice when defective[44] and *Dctd* that has altered genome interactions in fat morbidities[45] and increased SNPs in childhood obesity[46] (Fig. 5d). Notably, the *Cpe* gene was directly next to rather than overlapping with a newly formed LAD in adipogenesis, suggesting that promoters can be specifically targeted by this regulation.

Proteins encoded by DR genes normally released from the NE and activated in adipogenesis that failed to do so in the Tmem120a knockdown include Fumarate hydratase (Fh1) that is important for respiration[47], Parm1 that is associated with insulin resistance[48], Jazf1 that is associated with type 2 diabetes[49], lipid metabolism proteins

Pla2g12a and Ak4[50,51,52], and adipokine Sema3c[53] (Fig. 5e). Expression of these genes increased in differentiated adipocytes, but this was mitigated with *Tmem120a* knockdown. Thus, multiple genes involved in different aspects of fat metabolism were reduced upon loss of Tmem120a. The repositioning of both *Dctd* and *Fh1* was confirmed by FISH (Fig. 5f and Supplementary Fig. 5c).

Ad-Tmem120a$^{-/-}$ WAT Shows Impairment of Tmem120a Regulated Gene–repositioning Observed in 3T3-L1 Adipogenesis

We next tested if *Ad-Tmem120a*$^{-/-}$ mice recapitulated gene repositioning changes of the 3T3-L1 system. FISH was performed on paraffin-embedded and sectioned iWAT from wild-type or knockout animals. All genes tested confirmed the Tmem120a dependence of repositioning. Anti-adipogenic *Dctd*, that repositioned to a LAD during 3T3-L1 adipogenesis, failed to be recruited to the NE in iWAT from *Ad-Tmem120a*$^{-/-}$ mice (Fig. 5g and Supplementary Fig. 5d). Moving in the opposite direction, *Fh1* that is normally released from the NE during 3T3-L1 adipogenesis, was away from the NE in control littermate iWAT; however, in iWAT from the *Ad-Tmem120a*$^{-/-}$ mice this gene was at the NE as in the undifferentiated 3T3-L1 pre-adipocytes (Fig. 5g; Supplementary Fig. d).

As genes associated with myogenesis were also highlighted by both DamID and expression data, we similarly tested genes encoding muscle myosin heavy chain 1 and 2 (*Myh1* and *Myh2*), calcium-activated chloride channel Ano5 that is mutated in limb-girdle muscular dystrophy[54], Myo18b, and Unc13c that are all recruited to the NE and repressed in 3T3-L1 adipogenesis (Supplementary Fig. 5d,e and Supplementary Tables 3 and 4). These genes were in the nuclear interior in *Ad-Tmem120a*$^{-/-}$ mice, indicating that they had failed to be recruited to the NE (Fig. 5g and Supplementary Fig. 5f,g). All tested genes exhibited corresponding expression changes in the mice (Supplementary Tables 3 and 4).

a

	n	% genome	coverage Mb	min Kb	max Kb	mean Kb	median Kb
LADs pre-adip	3914	44.9	1192.5	15.0	10.5	304.7	83.2
LADs adip	2542	45.1	1197.9	15.0	10.0	471.2	103.1
LADs kd A adip	5723	43.8	1163.9	15.0	5.8	203.4	59.1
LADs kd AB adip	6971	43.7	1161.4	15.0	4.1	166.6	60.7
DR pre-adip (PI)	2021	3.9	103.2	8.0	501.0	51.1	37.1
DR adip (IP)	1808	4.1	108.9	8.1	571.6	60.2	40.6

b

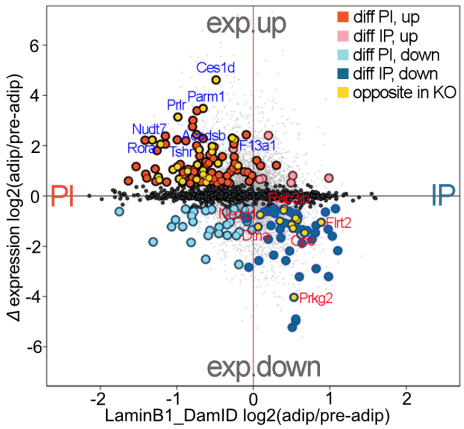

c

	down	up	no change
II	2207	2336	10657
PI	36	94	974
IP	56	8	513
PP	20	30	3197

d

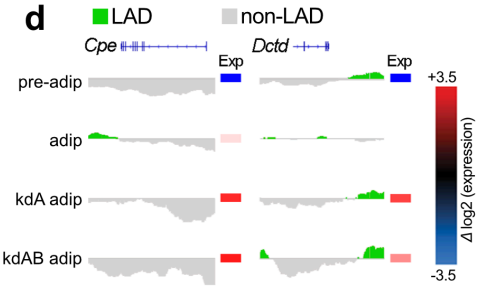

e

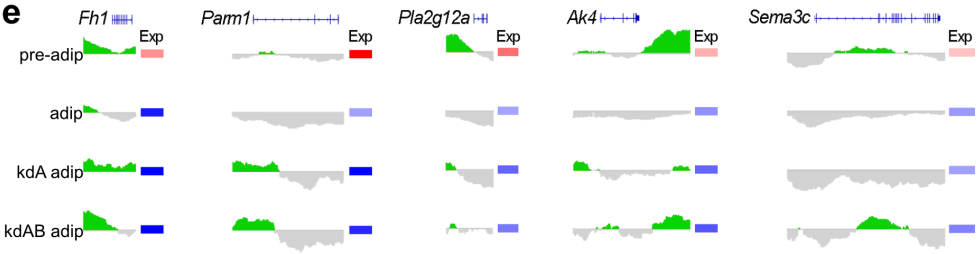

f

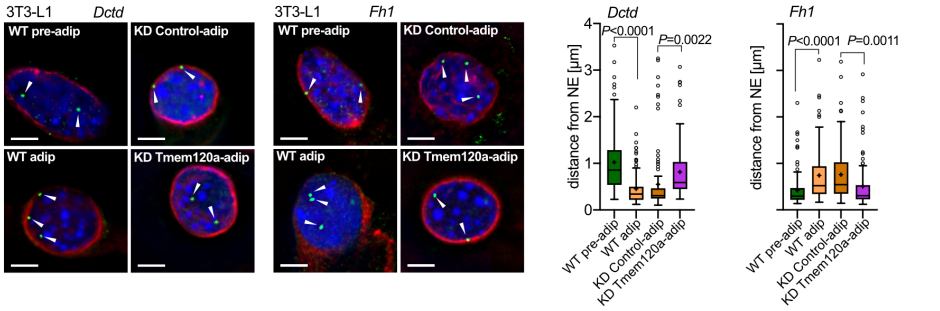

g

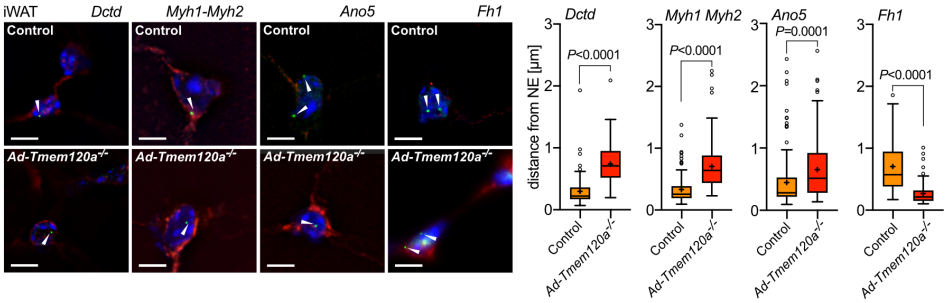

Fig. 5. DamID and Transcriptomics Analysis Reveals Tmem120a Contributes to Gene Regulation in Adipocyte Differentiation

a, LaminB1-DamID on 3T3-L1 preadipocytes and adipocytes, upon *Tmem120a* knockdown as well as *Tmem120a* and *b* double knockdown. Table shows metrics for lamina associated domains (LADs). **b**, Correlation of gene expression and gene positioning shown as distribution scatter plot of genes differentially expressed during adipogenesis (adip/pre-adip) and LamB1-DamID values, PI – genes moving from periphery to nuclear interion, IP – genes moving toward nuclear periphery. **c**, Table showing numbers of genes changing expression upon being repositioned between nuclear interior "I" and nuclear periphery "P" during adipogenesis. **d** and **e**, Example DamID traces and expression changes of two genes being recruited to the NE (IP) upon differentiation that failed to reposition with *Tmem120* knockdown (**d**), and examples for the opposite direction (PI) (**e**). **f** and **g**, FISH in 3T3_L1 system for the *Dctd* and *Fh1* genes in green with white arrow heads during wild-type adipogenesis and in the *Tmem120a* knockdown (**f**) and in mouse iWAT from control animals vs *Ad-Tmem120a*$^{-/-}$ detecting the position of the *Dctd, Myh1/Myh2, Ano5* and *Fh1* genes (**g**); scale bars: 5 μm; distance from NE quantification is shown as box plot means SEM, cross on the box represents median. *P* values: by unpaired Student's *t*-test. See also Supplementary Fig. 5.

Enhancers and Regulatory RNAs Were Also Altered in *Ad-Tmem120a*$^{-/-}$ Mice

While the above genes changed both expression and position in the mice, some genes with changed expression in the knockout did not correspondingly change position. We previously found that many enhancers are recruited to or released from LADs during lymphocyte activation[55]. Therefore, we searched DRs for predicted enhancers, finding that a third of all pre-adipocyte enhancers that exhibited functional repression during adipogenesis were recruited to the NE while 31 enhancers that became activated in adipocytes were released from the NE (Fig. 6a). We tested the positioning of one of these predicted to act on the *Klf9* gene that is in a pre-adipocyte LAD that disappears upon differentiation, yet is retained in adipocytes knocked down for Tmem120a. FISH confirmed this predicted enhancer releases from the NE during adipogenesis (Fig. 6b).

Another way to explain Tmem120a effects on gene expression absent positional changes in the affected genes is changes in regulatory RNAs. Indeed, RNA-Seq on the mouse iWAT indicated changes in lncRNA levels (Supplementary Table 2), with H19, a lncRNA involved in skeletal muscle and heart differentiation[56] upregulated 3.2-fold in *Ad-Tmem120a*$^{-/-}$ mice compared to control littermates (Fig. 6c). This raised the possibility of other indirect effects on gene expression from changes to other regulatory RNAs.

Levels of 717 miRNAs were determined in control and knockout mouse iWAT by high-throughput qPCR (Fig. 6d and Supplementary Table 5). Of 79 upregulated miRNAs, 45 had relevant links to the *Ad-Tmem120a*$^{-/-}$ pathology. Links were found for 19 (24.1%) to myogenesis, 9 (11.4%) to adipogenesis, and 25 (31.6%) to insulin resistance or obesity (Supplementary Table 5). miR-339-3p, the most upregulated, was increased over 20-fold and affects Akt signalling pathways important for insulin regulation[57,58]. The next most upregulated were miR-1 at 18-fold and miR-133a at 9.8-fold that work together to promote muscle differentiation[59]; hence upregulation of these miRNAs may enhance de-repression of myogenic pathways. They are also linked to

diabetes and miR-133a is additionally involved in WAT browning and so could explain BAT fat accumulation in *Ad-Tmem120a*$^{-/-}$ mice.

In the opposite direction, of 81 miRNAs with decreased levels, 60 had links to *Ad-Tmem120a*$^{-/-}$ pathology. These connections included 10 miRNAs (12.3%) related to myogenesis, 30 (37%) to adipogenesis, and 37 (45.7%) to insulin resistance or obesity (Supplementary Table S5). The strongest decrease was 9.2-fold and the average fold change was 3.3-fold. Of particular note, knockdown of miR-27b, miR-92a, miR-155, and miR-150 have all been shown to enhance browning/ beiging[60,61,62,63], one of the *Ad-Tmem120a*$^{-/-}$ pathologies. Also, miR-322, miR-15b, miR-342-5p, and miR-16 are all pro-adipogenic[64,65,66]; so their reduction is consistent with the pathology. Finally, miR-151-3p, miR-466f, miR-139-5p, miR-219, miR-29b, miR-25, and miR-370 are all linked to diabetes[67,68,69,70,71,72,73], consistent with the inability to clear glucose, insulin resistance, and elevated insulin in *Ad-Tmem120a*$^{-/-}$ mice.

Of these 160 mis-expressed miRNAs, 67% were found in serum from ADicerKO mouse, a lipodystrophic mouse, and 9 were misregulated in serum from human lipodystrophy patients[74] (Supplementary Table 5). Moreover, 33 of the loci encoding them were under positional regulation according to the DamID data (Supplementary Table 5). Surprisingly, a majority of those under Tmem120a positional regulation did not change position during normal adipocyte differentiation, but all of those normally repositioning in adipogenesis failed to reposition in *Tmem120a* knockdown cells. Examples include the loci encoding miR-201, miR-216a, and miR-710 that increase at the NE during adipogenesis and fail to do so in *Tmem120a* and *Tmem120*/*Tmem120b* knockdowns, corresponding to their increased expression (Fig. 6e). miR-201 may contribute to fatty acid metabolism as it targets very-long-chain enoyl-CoA reductase[75] while miR-216a is a risk biomarker for atherosclerosis in paediatric patients with diabetes[76]. In the opposite direction, the loci encoding miR-340 and miR-467 were released from the NE in adipogenesis and failed to release with *Tmem120* knockdown, corresponding with their reduced levels (Fig. 6e). miR-340 is

linked to gestational obesity[77] and type 2 diabetes[78]. The locus encoding miR-181a exhibited an intermediate effect. It was recruited to the NE during normal adipogenesis, but, when *Tmem120a* was knocked down, the LAD it occurs in was shortened. In the double knockdown the LAD completely disappeared. In the mice expression of the miRNA locus was increased even though *Tmem120a* alone was knocked out. miR181a appears to be important for adipogenesis in both porcine[79] and 3T3-L1 mouse models[80] and interestingly, considering Tmem120a effects on circadian switching for oxidative metabolism, it modulates circadian rhythm in adipose-derived stromal cells[81]. Some repositioning changes were harder to interpret. For example, miR-690 remained in a LAD during normal adipogenesis yet was released from the NE with *Tmem120a* knockdown but not the double knockdown (Fig. 6e). miR-690 regulates induced pluripotent stem cell differentiation into insulin-producing cells[82] and is downregulated in high glucose conditions[83].

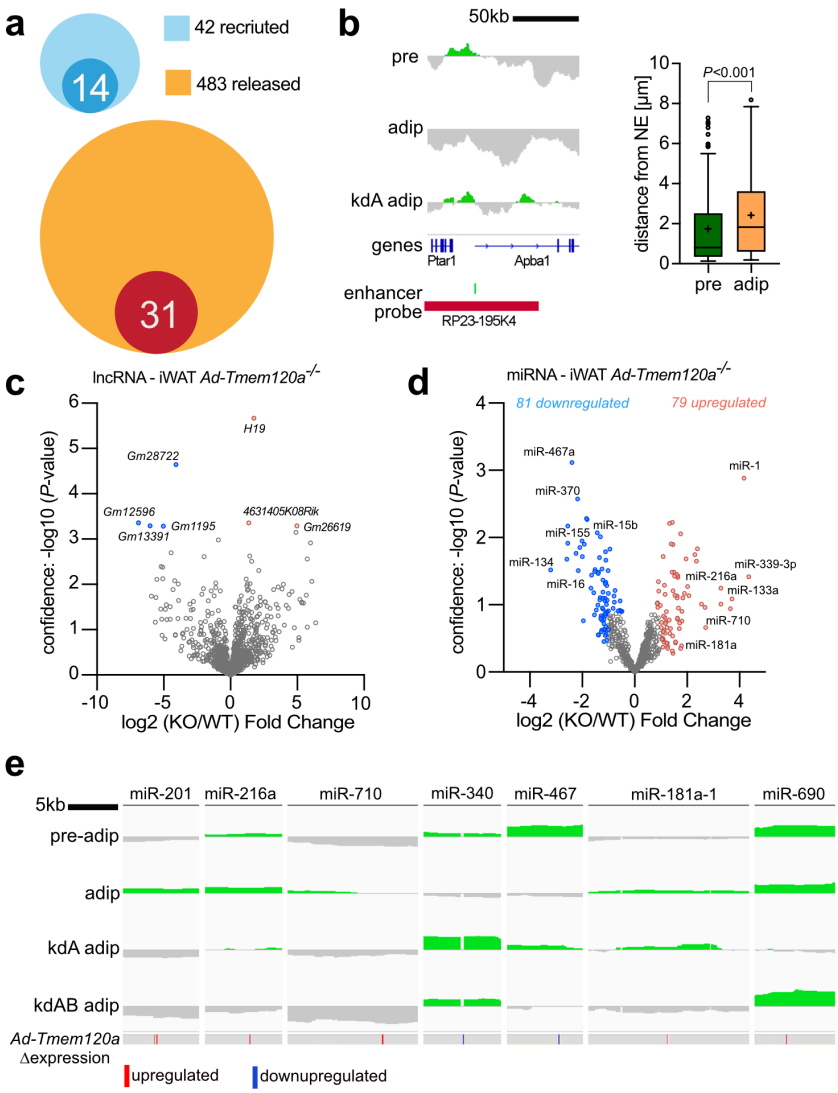

Fig. 6. Enhancers and Regulatory RNAs Under NE Positional Control

a, Venn diagrams showing proportion of predicted adipogenic enhancers that become lost during adipogenesis – recruited to NE (light blue) or new adipocyte enhancers – released from NE (yellow). Dark blue circle represents enhancers that fail to recruit to NE during adipogenesis in Tmem120a KD 3T3-L1 cells. Red circle represents enhancers that fail to release form NE during Tmem120a KD 3T3-L1 differentiation. **b**, DamID trace and FISH distance quantification of the Klf9 enhancer. **c**, Volcano plot showing expression of lncRNA, highlighting strong upregulation of the H19 expression in *Ad-Tmem120a*$^{-/-}$ iWAT. **d**, Volcano plot of differentially expressed miRNAs in inguinal subcutaneous adipose tissue (iWAT). **e**, DamID traces showing the position of miRNA-encoding loci with respect to changing LADs and their expression change in the knockout mouse. Blue, downregulated; red, upregulated.

Gene Mispositioning of *Ad-Tmem120a*$^{-/-}$ Mice Is Recapitulated in Human Partial Lipodystrophy Patients

As Tmem120a is in the NE and *Ad-Tmem120a*$^{-/-}$ mice had a latent lipodystrophy pathology, we postulated that TMEM120A might play a mediating role in NE laminA-linked FPLD2. If so, the gene mispositioning we observed in *Ad-*

Tmem120a$^{-/-}$ mice might also occur in human FPLD2 patients. Therefore, human FISH probes were used to test for positioning of 4 equivalent loci in human FPLD2 patient cells. Pre-adipocytes were isolated from neck fat biopsies from two FPLD2 patients and a healthy control and differentiated *in vitro*. As the strongest gene expression changes in the mouse were for myogenic genes, we chose 5 muscle genes that normally reposition from the nuclear interior to the NE in mouse adipogenesis and failed to reposition in the *Ad-Tmem120a*$^{-/-}$ mice corresponding to their derepression in mouse iWAT: *MYH1*, *MYH2*, *ANO5*, *TRIM55*, and *MYO18B*. We first tested these for repositioning in human adipogenesis as there is commonly incomplete correspondence between mouse and human in genome organisation studies due to synteny differences and the fact that sometimes a different variant of the same protein family is used for a particular function between the two species. Because the *MYH1* and *MYH2* genes are adjacent to one another a single BAC probe was used to cover both genes. *MYH1*, *MYH2*, *ANO5*, *TRIM55* all repositioned as expected, but *MYO18B* was positioned internally in both the pre-adipocytes and adipocytes in the control and so did not reposition and was not followed further (Fig. 7a-d). When the remaining genes that all similarly repositioned between the nuclear interior and NE during adipogenesis in both mouse and human were tested in the FPLD2 patient cells, all four genes failed to reposition in the lipodystrophy patients upon adipogenic differentiation while they did in the controls (Fig. 7a-c).

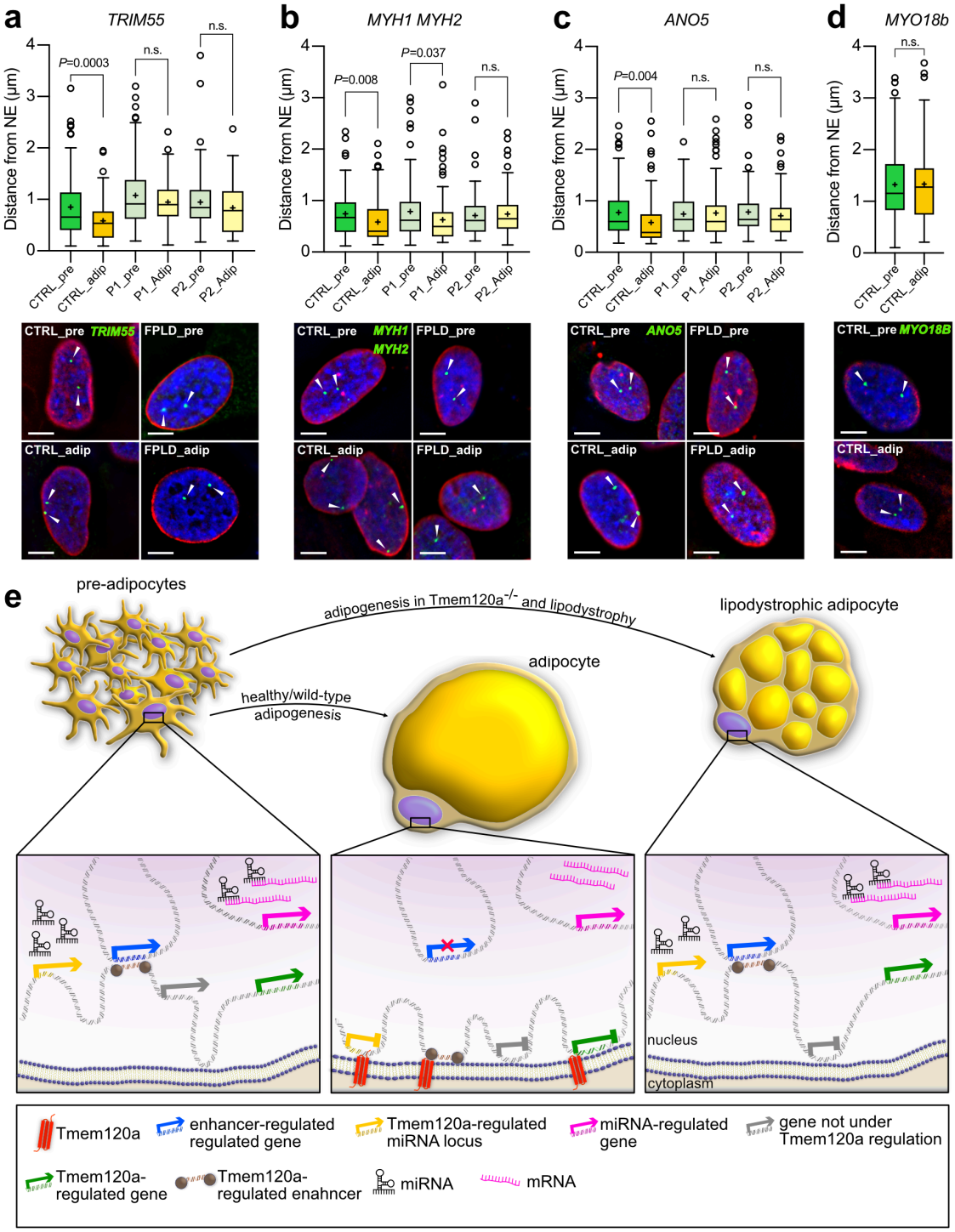

Fig. 7. Genes Misregulated in *Ad-Tmem120a*$^{-/-}$ Mice Are Also Misregulated in Human Lipodystrophy Patients

a-d, Quantification and representative images of FISH for *TRIM55*, *MYH1/MYH2*, *ANO5*, and *MYO18b* gene loci distance from the NE in human primary SVF cells before and after induction of adipogenesis: CTRL, healthy donor; pre, preadipocytes; adip, adipocytes; P1 and P2 stands for patient 1 and patient 2 respectively. Cells are from anonymised FPLD patients donating tissue. **e**, Model of genome organisation role in adipogenesis and lipodystrophy. In preadipocytes, some muscle genes (e.g., *Myh1*) are in the nuclear interior that need to be strongly shut off in adipocytes and so are recruited to the NE when Tmem120a is expressed during adipogenesis. In the opposite direction, some genes are released from the NE and become activated when Tmem120a is expressed; however, in the absence of Tmem120a they remain at the NE and their expression is reduced compared to wild-type adipocytes. Enhancers and miRNA-encoding loci are similarly under Tmem120a positional and expression regulation. *Ad-Tmem120a*$^{-/-}$ adipocytes parallel human FPLD2 patients in that the normal repositioning of several genes that takes place during adipogenesis is disrupted with a concomitant change in expression.

DISCUSSION

Tmem120a disruption in mice yields a latent lipodystrophy pathology resembling in many ways laminA-linked FPLD2, including a pronounced gender dimorphism of currently unknown molecular etiology. The correspondence between the mispositioning of several specific genes, enhancers and miRNAs supporting adipocyte differentiation with concomitant changes in expression, metabolism, and mouse pathology suggests that the latent lipodystrophy pathology arises due to disruption of fat-specific patterns of genome organisation. That similar genome organisation defects occurred in human FPLD2 caused by laminA mutation raises the possibility that TMEM120A might mediate the fat-specificity of this disorder as laminA is widely expressed. The potential of TMEM120A to contribute to human adiposity disorders is increased by recent findings of point mutations in muscle-specific NETs with parallel genome-organizing functions in Emery-Dreyfuss muscular dystrophy[84] that similarly has variants caused by laminA mutations. Thus, these findings have ramifications for spatial genome organisation, fat development and metabolism, and human disease.

The latent lipodystrophy pathology of *Ad-Tmem120a*$^{-/-}$ mice is more similar in some ways to human FPLD2 than the laminA FPLD2 mouse model expressing a human laminA R482Q transgene from the aP2 promoter[85]. Both our *Ad-Tmem120a*$^{-/-}$ mice and the aP2-R482Q mice exhibited insulin resistance, glucose intolerance, and fat loss with a depot-specific pattern consistent with human FPLD2. The aP2-R482Q mice more closely parallel human FPLD2 in having hyperlipidemia and hepatic steatosis due to accumulation of lipids in non-adipose tissues. In contrast, *Ad-Tmem120a*$^{-/-}$ mice had no hyperlipidemia, no increase in hepatic lipid droplet size, and no significant increase in liver mass. This may indicate a distinct Tmem120a-linked lipodystrophy pathology with translational significance given a recent report that hepatic steatosis occurs in only ~10% of lipodystrophy patients[30] and that hyperlipidemia is variable in the human disorder[32]. The implication for the latter

argument is that laminA mutation effects on liver are largely direct, as opposed to indirect from lipids that cannot be processed by fat stores. Intriguingly, our model may eventually illuminate mechanisms underpinning sex-specificity of lipodystrophy as Ad-Tmem120a knockout mice had more pronounced effects in females while the laminA mutant line yielded pathologies, including the hepatic steatosis, principally in males[86]. Furthermore, in FPLD2 loss of subcutaneous fat from the extremities, trunk, and gluteal region is partly countered by increased fat in the neck (where adult human BAT concentrates) and increased muscle mass. The laminA model had a severe reduction in brown subscapular fat pads and no significant increase in lean mass. In this, our adipose tissue specific *Tmem120a* knockout mice were closer to the human disorder having both maintained BAT mass and increased skeletal muscle mass.

We speculate that the increased fat accumulation in *Ad-Tmem120a*$^{-/-}$ BAT parallels the fat accumulation in the necks of FPLD2 patients[87,88], especially as adipose tissue browning is observed in FPLD2[89]. BAT stores less lipid, has more mitochondria and can dissipate energy as heat without ATP generation whereas WAT is less efficient at converting lipid to energy but more efficient at lipid storage[90,91]. Thus, the accumulation of fat in BAT suggests a deficiency in BAT metabolic function that could be accounted for by both the repressed genes and altered miRNAs. Furthermore, several of the altered miRNAs have reported functions in beiging[60,61,62,63] and this could also explain the change in BAT function.

We posit that the increased lean/muscle mass in our model and in human FPLD2[87,88] could be accounted for by the known functions on muscle of several of the miRNAs elevated in our *Ad-Tmem120a*$^{-/-}$ mice such as miR-1 and miR-133a that work together to promote muscle differentiation[59]. Many of the pro-myogenic miRNAs affected by Tmem120a deficiency were found in serum of human patients with various fat disorders[74] suggesting a potential adipocyte-muscle paracrine mechanism driving increased muscle mass.

That miRNA levels, fat enhancers, and relevant gene expression correlated with genome regions moving between the NE and nuclear interior suggests that the mechanism behind our mouse pathology is disruption of fat-specific genome organisation. The notion that gene positioning influences gene regulation has been criticised because only a fraction of all the genes that change position also change expression and of this fraction only ~70% change expression in the expected direction[18,42]. The favoured explanation for these poor correlations is that multiple adjacent genes reposition together, but only those with transcriptional regulators present change expression[18]. Our new data can better explain those changing expression in the unexpected direction through enhancers and regulatory RNA-encoding genome regions that are also under Tmem120a positional control (Fig. 7e). This argument is the stronger when considering that >75% of the altered miRNAs had functions influencing fat or muscle.

A recent report argued that *Tmem120a* encodes a brain ion channel named TACAN[25]. It is possible that the much higher molecular weight isoform in brain we previously reported[20] has a distinct function. However, it is also possible that a genome organisation defect could largely explain their results as ion channels Cacna1s, Clca2, Slco1a5, Ano5, Tmem150c, ATP2a1, Kcnv2, Fxyd2, Slc4a8, and Kcnh8 were all misregulated in our model. Notably, Atp2a1 is a Ca2+ ATPase pump that regulates glucose transport and is linked to diabetes[92,93], further linking Tmem120a indirectly to ion transport and directly to adipocyte function. Our data is further supported by 5 different groups finding human and mouse TMEM120A links to adiposity[20,21,22,23,24].

Cumulatively, these data suggest a new paradigm for genome organisation defects in disease where multiple minor changes in expression can yield a disease phenotype as opposed to blocking of one central pathway. A few genes from different pathways were reduced ~10-fold while many genes were reduced only a few fold in our knockout, yet it yielded a latent lipodystrophy pathology without any major adiposity genes/pathways being strongly shut down. Such minor changes in multiple genes

would be likely to reduce overall efficiency of metabolic function, consistent with the later presentation of NE-linked lipodystrophies long after tissue differentiation and when metabolic loads are increased[94]. Obesity and other metabolic disorders are increasing throughout the world with age-standardized diabetes in men increasing from 4.3% in 1980 to 9% in 2014[95]. Our findings highlight TMEM120A as a potential target/model for these disorders due to the large range of fat metabolic genes it affects and our finding of minimal phenotype in animals on the low-fat diet supports the clinically favoured approach of caloric restriction to improve metabolic parameters in lipodystrophy[96]. Further work dissecting out TMEM120A critical miRNA targets could potentially enable miRNA therapies targeting separately its muscle mass function for muscle disorders and its fat metabolic functions for obesity.

ACKNOWLEDGEMENTS

We thank Sue Shackleton (Leicester) for helping us establish the 3T3-L1 system and David Kelly for assistance with image analysis. We also thank Honours student Jeremy Stewart who did the first experiments indicating the project was viable. D.G.B. was supported by a Darwin Trust Studentship and this work was principally supported by Wellcome Senior Research Fellowship 095209, Medical Research Council MR/R018073, and Muscular Dystrophy UK 18GRO-PG24-0248 to E.C.S., Wellcome Trust New Investigator Award 100981/Z/13/Z to N.M.M. and Wellcome Trust Centre for Cell Biology core funding (092076).

AUTHOR CONTRIBUTIONS

RC, DGB, RNC, MS, AS, CRD conducted and designed experiments. GL provided patient samples. JIH, SW conducted bioinformatic analysis. ECS, RC and NMM wrote manuscript.

DECLARATION OF INTERESTS

The authors have no conflicts of interests to declare.

SUPPLEMENTARY INFORMATION

Supplementary information includes 3 figures and 5 Tables and can be found online at: https://data.mendeley.com/datasets/8hgntm9x3w/draft?a=5fef1d20-884f-4237-8686-1ecb1c02e47c

Methods

Animals

A conditional *Tmem120a* knockout mouse was generated by Taconic. The strategy was targeted to the NCBI transcript NM_172541.2. A targeting vector was generated using BAC clones from the C57BL/6J RPCIB-731 BAC library and was transfected into the Taconic C57BL/6N Tac ES cell line. The targeting vector consisted of exons 2 and 3 region flanked by *loxP* sites as well as the puromycin selection cassette designed to be removed after *in vivo* Flp-mediated recombination (Supplementary Fig. S1A). Recombination of the targeting vector was confirmed by Southern blotting (Supplementary Fig. S1B). Conditional knockout homozygotes (*loxP/loxP)* were crossed with an Adipoq-Cre deletor mouse carrying promoter for adiponectin followed by *Cre* recombinase transgene, kind gift from professor Evan Rosen (RRID_IMSR_JAX:028020), described in[27]. Adipoq-Cre deletor mouse was chosen to obtain expression of Cre recombinase in mature adipocytes and to avoid expression in brain, macrophages and muscles observed in other models of adipose tissue specific Cre systems[28,29]. Genotyping for *loxP* sites was performed by PCR with primers flanking two *loxP* sites, F1 5' CTTTCAGGCTGGGTAGGTAGG, R1 5' GGGCGTCTGAATTCTAAGTGG and F2 5' GAGTTCAAAGTTAGCCTAGTCAGC, R2 5' TCCAGAAGGTGGTATCAGATCC. To genotype Adipoq-Cre mice, detection of the transgene was performed by PCR and use of the following pairs of primers: *Cre* forward 5' GCGGTCTGGCAGTAAAAACTATC, reverse 5'

GTGAAACAGCATTGCTGTCACTT, in combination with the internal positive control (*Il2* gene): forward 5' CTAGGCCACAGAATTGAAAGATCT, reverse 5' GTAGGTGGAAATTCTAGCATCATCC. Animals were kept in an air-conditioned room in 12h light and dark cycles (light on 7 am) with *ad libitum* access to water and food. Experiments involving animals were approved by the University of Edinburgh ethical committee and Home Office UK under project licenses granted to ECS and NMM.

In Vitro Adipocyte Differentiation and Stable shRNA Lines

3T3-L1 (RRID_0123) cells were maintained in high glucose DMEM (SIGMA) supplemented with 10% fetal bovine serum (FBS), MEM non-essential amino acids, 1 mM Sodium Pyruvate, 100 µg/µl penicillin and 100 µg/µl streptomycin sulfate. Cells were plated at ~10% confluency and always split by 60% confluency to maintain differentiation capacity. Adipogenesis was induced two days post-confluency by replacing growth medium with induction medium containing 0.5 µM insulin, 1 µM dexamethasone, 0.5 mM 3-isobutyl-1-methylxanthine (IBMX), and 1 µM rosiglitazone. Induction medium was replaced after two days with maintenance medium containing growth medium supplemented with insulin and rosiglitazone only. Stable 3T3-L1 shRNA lines for knocking down of *Tmem120a* and *Tmem120b* genes were described in[20].

Human preadipocytes

Human preadipocytes from healthy donors and familial partial lipodystrophy type 2 patients were from the BioLaM biobank (Rizzoli Orthopedic Institute Ethical Committee approval, No. 0018250–2016) located at the CNR Institute of Molecular Genetics Unit of Bologna. Neck adipose tissue of patients undergoing aesthetic surgery had been collected according to local and EU ethical rules. Pre-adipocyte cultures had been established from the stromal vascular fraction and cultured in D-MEM plus 20% Fetal

Bovine Serum and antibiotics. Cells were differentiated into adipocytes as described previously[89].

Dissections and Histology

Animals were fasting for 16 h, measured and terminated by cervical dislocation. Blood was collected for plasma biochemistry and dissected tissues were weighted and snap-frozen in liquid nitrogen for RNA isolation or fixed in 10% paraformaldehyde (PFA) for 24h at 4°C for histology and fluorescent *in situ* hybridization. PFA-fixed adipose tissue pads were processed in 70% ethanol for 24 h and embedded in paraffin. 4 µm thick sections of adipose tissue were stained by hematoxylin and eosin by the standard protocol for measurement of the lipid droplet size. To measure lipid droplet size in liver, tissues were embedded in OCT compound (*Tissue-Tek*), frozen on dry ice, cut into 4 µm sections and stained with hematoxylin and eosin. Pictures were taken at 40x magnification with the Axio Imager microscope (*Zeiss*) and Qimaging Micropublisher 3.3 camera (*Digital Imaging Systems*). Lipid droplet area was measured by Image J (NIH, USA) software with the Adipocytes Tolls plugin (*Montpellier Ressources Imagerie*). Three animals per group were analysed with 10 random area pictures per animal.

Metabolic assessment

3-4 months old mice were subjected to dietary intervention. In high fat diet experiments, animals were fed a 58% kcal from fat, 25.5% kcal from carbohydrates and 16.4% kcal from protein diet (*Research Diets,* cat. D12331). Low-fat diet delivered 10.5% kcal from fat, 73% kcal from carbohydrates and 16.4% kcal from proteins (*Research Diets,* cat. D12328). To assess glucose metabolism, mice underwent glucose tolerance test (GTT). Briefly, 12 h fasting animals were given a bolus intraperitoneal injection of 20% D-glucose solution (*SIGMA*) in saline at 2 mg/g bodyweight. Glucose level was measured in the blood from a tail venesection at time

0, 15, 30, 60, 120 min using an Accu-Check, Aviva Nano, (*Roche*) glucose monitor. To evaluate whole body insulin sensitivity, an insulin tolerance test (ITT) was performed. After a 6 hour fast, animals were injected with a bolus of 0.2 U/mL insulin (Humulin S, *Eli Lilly and Company Ltd.*) in saline to deliver 1 mU/g bodyweight. Glucose level during ITT was measured at the same time intervals as in GTT.

Indirect Calorimetry and TD-NMR

To evaluate energy expenditure, respiratory exchange ratio (CO_2/O_2), water consumption, food intake, activity (X-Y-Z), was measured in indirect calorimetry chambers (PhenoMaster, *TSE Systems*). Single caged mice were analyzed for at least 48h after at least 24h of acclimation to their new cage. There was *ad libitum* access to water and food. Oxygen and carbon dioxide levels were measured in real-time by a set of sensors. Fat and lean mass was determined by TD-NMR (Live Mice Analyzer, The Minispec LF90II, *Bruker*). Energy expenditure is presented as Kcal/kg lean mass/min.

Plasma biology

Blood collected to an anticoagulant (EDTA) coated tubes was centrifuged in 4°C at 2800 rpm for 10 min and supernatant collected and snap-frozen in liquid nitrogen. High Molecular Weight (HMW) Adiponectin ELISA (*ALPCO,* cat. 47-ADPMS-E01, RRID:AB_2801466) was used according to manufacturer instruction. HMW fraction was used as it is a better indicator of insulin sensitivity for health and disease status monitoring[97]. Insulin and Leptin ELISA were used according to manufacturer's instructions (*Chrystal Chem Inc.*, ref. 90080 - RRID:AB_2783626 and 90030 - RRID:AB_2722664 respectively). To measure the level of triglycerides LabAssay Triglyceride kit was used according to manufacturer instructions (*Fujifilm Wako Diagnostics,* cat. 290-63701). Non-esterified fatty acids (NEFA) levels were measured

by an enzymatic colorimetric assay (*Fujifilm Wako Diagnostics,* cat. HR Series NEFA-HR2, No. 99934691), using manufacturer manual.

Stromal Vascular Fraction (SVF) and adeno-associated virus (AAV)

To obtain primary, preadipocyte-rich cell population, stromal vascular fraction (SVF) cells were isolated from inguinal subcutaneous fat pads. Three-months-old mice, homozygous for *loxP/loxP* were terminated, fat pads removed and washed in PBS. Tissue was cut into 3-4 mm cubes and placed in digestion medium: KREB's Phosphate Buffer (118 mM NaCl, 5 mM KCl, 1.2 mM $MgSO_4$, 12 mM Na_2HPO_4, adjusted to pH 7.4 with 100 mM NaH_2PO_4) supplemented with 2 mg/mL collagenase I (*Gibco,* cat. 17018-029,), 1% Bovine Serum Albumin, 1 mg/mL glucose and 1.265 mM $CaCl_2$. Diced tissue was incubated for 1 h at 37ºC with slow agitation. The reaction was stopped by adding SVF maintenance media (DMEM/F12 media with 10% FBS, 100 U/mL penicillin, 100 µg/mL and 2 mM L-Glutamine). Released cells were immediately centrifuged at 1500 rpm for 5 min to separate SVF cells from mature adipocytes. The SVF cells in the pellet were resuspended in the maintenance media, passed through a 70 µm cell strainer, centrifuged again, resuspended and plated in fresh SVF maintenance media at a concentration of 500 cells/cm^2. SVF cells were differentiated into adipocytes under the same protocol as used for 3T3-L1 cells described above. To achieve *Tmem120a* knockout in primary SVF cells *loxP* sites recombination was induced *in vitro* by the delivery of the *Cre* recombinase gene fused with GFP in AAV virus (RRID:Addgene_49056). As a control AAV with the GFP-only construct was used (RRID:Addgene_49055). Virus particles were produced in HEK293FT (RRID_6911) cells by co-transfection of AAV plasmids with the helper plasmid pAdDeltaF6 (RRID:Addgene_112867) and AAV packaging plasmid expressing Rep2/Cap5 genes for production of serotype 5 – pAAV2/5 (RRID:Addgene_104964).

Mitochondrial Respiration (Stress Test and Substrate Dependency)

Oxygen consumption rates (OCR) from differentiated SVF cells were analyzed by the Seahorse XF24 Extracellular Flux Analyzer - (*Agilent Technologies*). Cells were seeded, infected with AAV-Cre virus and differentiated into adipocytes on V28 Seahorse plates. Until fully differentiated (day 7-8), cells were cultured at 37°C with 5% O_2 and 5% CO_2 atmosphere. 30 min before the experiment, maintenance media was replaced with XF base medium (*Agilent Technologies* cat. 103193-100) supplemented with 2 mM L-glutamine, 2 mM pyruvate and 10 mM glucose for pre-incubation in a non-CO_2 atmosphere at 37°C to equilibrate the cells with the XF media. V28 plates were used because SVF cells are known to have higher respiration than other commonly cell types (e.g., fibroblasts, cancer cells) and these plates adjust the probe position so that the higher readings do not saturate the machine. Basal and maximal respiration, as well as ATP-linked and proton leak respiration, were determined with a mitochondrial stress test, using optimized drug concentrations. First, oxygen consumption rate (OCR) was measured three times for calculation of basal respiration, followed by an injection of 4 µM oligomycin to calculate respiration linked to ATP production. Next, 1 µM FCCP (respiratory uncoupler) was added for calculating maximal respiration. Finally, simultaneously, 1 µM of rotenone and 1 µM of antimycin A (blockers of electron transport chain complex I and III, respectively) were added to terminate mitochondrial respiration. That enabled the correction of basal and maximal respiration by subtraction of non-respiratory OCR. ATP linked respiration was calculated by the drop in OCR following oligomycin. Proton leak was calculated by subtracting ATP-linked respiration from basal respiration. Pyruvate dependency for respiration in *Tmem120a* knockout adipocytes was performed in the same assay media as mitochondrial stress assay. Briefly, after basal OCR measurement, 6 µM of mitochondrial pyruvate transporter inhibitor UK9055 (*Merck*, cat. 5048170001) were added to test if mitochondria have the capacity to utilize other substrates than pyruvate.

This was followed by 4 µM oligomycin, to test ATP- production-linked respiration in the absence of pyruvate. Next, 1 µM FCCP was added followed by the simultaneous injection 1 µM of rotenone and 1 µM of antimycin A. Dependency on pyruvate was defined as the difference between the OCR calculated from the vehicle and the UK5099-inhibited OCR for each parameter. Results of the experiments are presented as the oxygen consumption rates (OCR) in pmoles O_2 / min / total protein. Protein content in each well was evaluated by the SRB assay (Sulphorhodamine B, *SIGMA*, cat. S1402) as described elsewhere[98].

qPCR

For isolation of total RNA from cultured preadipocytes, adipocytes and mouse adipose tissue RNeasy Lipid Tissue Mini Kit was used (*Qiagen,* cat. 74804) following manufacturer instruction. Quality of obtained RNA was tested on the capillary electrophoresis machine (2100 Bioanalyzer, *Agilent*) and material with RIN ≥ 7.0 (RNA integrity number) was used for further applications. 1 µg of RNA was used for cDNA synthesis and qPCR reaction was performed in LightCycler480II instrument with SYBR Green I Master Mix (*Roche*) and with following primers: mouse *Tmem120a* forward: 5' GAAAACCAGATGAAAGAGCGC and *Tmem120a* reverse: 5' GTGAAGGAGATGACGATGAGG. Expression was normalized to mouse *Gapdh*: forward 5' CCTCGTCCCGTAGACAAAATG, reverse 5' TTGACTGTGCCGTTGAATTTG and mouse *Rsp29*: forward 5' GAGCCGACTCGTTCCTTT, reverse 5' TGTTCAGCCCGTATTTGC.

To assess the miRNA profile in subcutaneous adipose tissue semi-high throughput, qPCR based, miRNome profiler was used, following manufacturer instructions (QuantiMir, *System Biosciences*, cat. RA670A-1). To acquire the miRNA-enriched RNA fraction from adipose tissue miRNeasy Mini Kit was used (*Qiagen*, cat. 217004), accordingly to producer manual in LightCycler480II instrument with SYBR Green I Master Mix. Experiments were performed in 5 biological replicates. Data were

analysed in R as per BioConductor HTqPCR package[99]. Briefly, Ct values were normalized per plate to the geometric mean of a set of provided house-keeping genes, and then normalized per sample using the 'quantile' function. Statistics were calculated using Limma[100] and miRNA genes were ranked by their p-values. We selected both genes that ranked in the top 15%, and those that were differentially expressed 2-fold or more and used the combined set for downstream analysis.

RNA-seq

Total RNA library was constructed with the TruSeq Stranded Total RNA Gold kit (*Illumina*, cat. 20020598), which is a ribosomal depletion-based kit. The RNA-seq experiment was executed by the North Texas Genome Centre at the University of Texas (Arlington, US), in the NovaSeq6000 machine, generating sequence dept of approximately 120M+120M (paired) reads. 150bp paired-end reads were aligned to the mouse mm9 assembly using STAR (v2.5.3.a, RRID:SCR_015899). The resulting alignments were filtered for reads that were properly paired, uniquely mapped and outwit blacklisted regions in the mm9 genome using BEDtools (v2.2.7, RRID:SCR_006646) and SAMtools (v1.9, RRID:SCR_002105). Pseudo alignment of read to transcripts was performed with Salmon (v0.13.1, RRID:SCR_017036) using cDNA and non-coding RNA sequences obtained from Ensembl NCBIM37.67 release. Read counts per gene were subsequently calculated using the R package tximport and Ensembl gene annotations (release 67). DESeq2 (v1.24.0) was used to find differentially expressed (DE) genes between pairs of samples, using an adjusted p-value of 0.1. Gene ontology (GO) analysis of the DE genes was performed with the web-based tool g:Profiler (RRID:SCR_006809) - https://biit.cs.ut.ee/gprofiler/gost[101]. Tissue-specific gene enrichment analysis was evaluated by the web tool TissueEnrich – https://tissueenrich.gdcb.iastate.edu[102].

Microarrays

3T3-L1 cells stably transfected with *Tmem120a*, *Tmem120a*/*Tmem120b*, or control non-target shRNAs were induced to differentiate for 6 days and RNA was extracted with Tri-Reagent (*Sigma*) according to the manufacturer's instructions. The RNA was converted to cRNA and labelled with biotin using the Illumina TotalPrep RNA Amplification Kit (*Ambion*, AMIL1791). For each analysis, at least two biological replicates were hybridised to Illumina whole-genome gene expression arrays (MouseWG-6 v2.0 BeadChip). Hybridisations were carried out by the Wellcome Trust Clinical Research Facility associated with the University of Edinburgh, using an Illumina Beadstation. Microarray data were quantile normalised and analysed in the R environment using the Bioconductor package Limma (RRID:SCR_010943)[100] using preadipocyte 3T3L1 cells as a reference. We selected differentially expressed transcripts using moderated F-statistics and adjusted for a false discovery rate of 5%[103]. A low intensity filter was applied, eliminating transcripts that do not reach a log2(signal) threshold of at least 6.5 in every sample, and we chose a low fold-difference cut-off of 1.4 (abs(log2 ratio)=0.5)

DamID

DamID was performed as in[39]. Briefly, 3T3-L1 pre-adipocytes or 6-day differentiated adipocytes +/- *Tmem120a* knockdown were transduced with either Dam-LaminB1- or Dam-only encoding lentiviruses and maintained for 3 days in the presence of 10 ug/ul protamine sulphate. At day 9 of differentiation genomic DNA from transduced cells was extracted and processed into libraries for next generation sequencing (Beijing Genomics). Sequenced reads were mapped to mouse mm9 genome and the $\log_2$(LaminB1/Dam) value determined for all genomic *DpnI* fragments. LADs and differential regions (IP and PI) were determined as described in Robson et al.[55]. Briefly, LADs were determined using the peak finder function in the BioConductor package DNAcopy (Seshan VE and Olshen A, 2016) *DNAcopy: DNA copy number data*

analysis. R package version 1.46.0, RRID:SCR_001905). IP and PI regions were then identified as regions displaying differential LADs.

3D Fluorescent *in situ* Hybridization (FISH) and gene positioning analysis

Probes for immuno-FISH on mouse cells and tissues were digoxigenin-labeled (Digoxigenin-11-UTP, *Sigma*) by nick translation from the following BAC or FOSMID clones covering genes loci: *Dctd* – RP23-441F24, *Fh1* – RP23-129O14, *Myh1* and *Myh2* – WI1-2202A13, *Ano5* – RP24-232N14, *Myo18b* – WI1-1944G3, *Unc13c* – RP24-294O13 (all probes from *BACPAC Genomics*). Human preadipocytes and adipocytes were FISH examined with the probes generated from the following BACs: TRIM*55* - RP11-164L7; *MYH1* and *MYH*2 - RP11-964J13; *ANO5* - RP11-116B7 and *MYO18B* - CH17-161F16 (all from *BACPAC Genomics*).

To prepare the probe for hybridisation approximately 200-600ng of labelled probe DNA was ethanol precipitated with the 5 µg of sheared salmon sperm DNA and 5 µg of mouse or human *Cot1* DNA (both from *Invitrogen*) and resuspended in hybridisation buffer (50% formamide, 2x SSC, 1% Tween20 and 10% dextran sulphate). After incubation at room temperature for 1 h, the dissolved probe was denatured at 80°C for 5 min, slowly re-annealed at the 0.1°C/s speed and kept at 37°C until the specimen was processed. 4 µm thick paraffin sections of adipose tissue were deparaffined by incubation in 60ºC for 15 min, then immersed in HistoChoice Clearing Agent (*Sigma*, cat. H2779) twice for 3 min. After that, tissues were rehydrated in decreasing concentrations of ethanol; 100%, 90% and 70%, 3 min each. Next, membranes were permeabilised in 20 µg/mL proteinase K solution in 50 mM Tris for 15 min. at 37ºC and slides rinsed 5x in distilled water. Subsequently, adipose tissue samples were permeabilised in 2M ice-cold acetic acid for 20 seconds and washed with water 5x. Similarly, cultured on coverslips adipocytes were fixed in 4% PFA for 10 min and permeabilised in 10 µg/mL proteinase K for 2 min at 37ºC. Preadipocytes were permeabilised in 0.5% Triton-X in PBS for 5 min. After permeabilisation tissue sections,

cultured pre- and adipocytes were treated in the same way. First, samples were blocked in 2% BSA and 0.1% Tween20 solution in PBS for 30 min at room temperature. Samples were then incubated with rabbit polyclonal primary antibody against LaminA[104] in blocking solution, followed by the donkey anti-rabbit 594Alexa Fluor secondary antibody (*Invitrogen,* RRID:AB_141637). After washing, immunofluorescence staining was fixed in 2% PFA for 1 min, samples were washed and incubated for 1 h with 100 µg/mL RNase A at 37ºC. Coverslips were then dehydrated in increasing concentrations of ethanol and denatured for 20 min in 70% formamide. After final dehydration labeled probe was loaded on the specimen and hybridised overnight at 37ºC. The unbound probe was then washed, hybridisation signal visualised by the 488Alexa Fluor-conjugated anti-digoxigenin antibodies (*Jackson ImmunoResearch,* RRID:AB_2339039) and nucleic acids were stained by Hoechst 33342 (*Thermo Scientific*). Finally, coverslips or slides were washed and mounted with Vectashield medium (*Vector Laboratories*). Image stacks (0.2 µm steps) were obtained using a TE-2000 microscope (*Nikon*) equipped with a 1.45 NA 100x objective, Sedat quad filter set, PIFOC Z-axis focus drive (*Physik Instruments*), and Prime 95B camera (*Photometrics*) run by MetaMorph (*Molecular Devices*) image acquisition software. Image stacks were deconvolved using AutoQuant X3 (*Media Cybernetics,* RRID:SCR_002465) software. Micrographs were saved from source programs as 12-bit .tiff files and prepared for figures using Affinity Designer (*Serif,* RRID:SCR_016952) and Photoshop (*Adobe*, RRID:SCR_014199). Loci signal distance from the NE was measured with the Imaris software (*Oxford Instruments,* RRID:SCR_007370). A minimum of 100 nuclei were analysed per animal/condition.

Bioinformatics analysis

Gene ontology analysis to test for over-representation using a hypergeometric test was performed using the Bioconductor package GOstats (RRID:SCR_008535)[105]. Only significantly over-represented GO terms (P<0.002) were considered for further

analysis. Biological Process terms associated with tissue remodelling, morphogenesis, development, and cell differentiation were grouped as “development”; terms involving localisation, cell locomotion, chemotaxis, migration and motility were grouped as “cell locomotion/ migration”; and terms including proliferation or growth were grouped as “cell growth/ proliferation”.

Materials Availability

All information and requests for resources should be directed to and will be fulfilled by the prof. Schirmer e.schirmer@ed.ac.uk. Mice generated in this study will be deposited in Charles River laboratories. Plasmids generated for this study will be deposited in Addgene. LaminA (3262) antibodies will be available upon request. Stable cell lines will be available upon request. Human samples might be available upon ethical approval. No other unique reagents were generated for this research.

Data and Code Availability

All datasets and bioinformatic algorithms will be available following publication of this study trough public repositories. RNA-Seq datasets have been made available through the Gene Expression Omnibus (GEO) repository at NCBI under accession number GSE147016 https://www.ncbi.nlm.nih.gov/geo/query/acc.cgi?acc=GSE147016, (note currently access requires password, but will be made completely public upon manuscript acceptance). DamID data is available through the Gene Expression Omnibus (GEO) repository at NCBI with accession number GSE150507 https://www.ncbi.nlm.nih.gov/geo/query/acc.cgi?acc=GSE150507, (note currently access requires password, but will be made completely public upon manuscript acceptance).

References:

1. Fadason T*, et al.* Physical Interactions and Expression Quantitative Traits Loci Identify Regulatory Connections for Obesity and Type 2 Diabetes Associated SNPs. *Front Genet* **8**, 150 (2017).

2. Frayling TM*, et al.* A common variant in the FTO gene is associated with body mass index and predisposes to childhood and adult obesity. *Science* **316**, 889-894 (2007).

3. Smemo S*, et al.* Obesity-associated variants within FTO form long-range functional connections with IRX3. *Nature* **507**, 371-375 (2014).

4. Guo Y*, et al.* CRISPR Inversion of CTCF Sites Alters Genome Topology and Enhancer/Promoter Function. *Cell* **162**, 900-910 (2015).

5. Lupianez DG*, et al.* Disruptions of topological chromatin domains cause pathogenic rewiring of gene-enhancer interactions. *Cell* **161**, 1012-1025 (2015).

6. Gonzalez-Sandoval A, Gasser SM. On TADs and LADs: Spatial Control Over Gene Expression. *Trends Genet* **32**, 485-495 (2016).

7. Cao H, Hegele RA. Nuclear lamin A/C R482Q mutation in Canadian kindreds with Dunnigan- type familial partial lipodystrophy. *Hum Mol Genet* **9**, 109-112 (2000).

8. Shackleton S*, et al.* LMNA, encoding lamin A/C, is mutated in partial lipodystrophy. *Nat Genet* **24**, 153-156 (2000).

9. Le Dour C*, et al.* A homozygous mutation of prelamin-A preventing its farnesylation and maturation leads to a severe lipodystrophic phenotype: new insights into the pathogenicity of nonfarnesylated prelamin-A. *J Clin Endocrinol Metab* **96**, E856-862 (2011).

10. Decaudain A*, et al.* New metabolic phenotypes in laminopathies: LMNA mutations in patients with severe metabolic syndrome. *J Clin Endocrinol Metab* **92**, 4835-4844 (2007).

11. Steinle NI*, et al.* Variation in the lamin A/C gene: associations with metabolic syndrome. *Arterioscler Thromb Vasc Biol* **24**, 1708-1713 (2004).

12. Owen KR*, et al.* Common variation in the LMNA gene (encoding lamin A/C) and type 2 diabetes: association analyses in 9,518 subjects. *Diabetes* **56**, 879-883 (2007).

13. Young J*, et al.* Type A insulin resistance syndrome revealing a novel lamin A mutation. *Diabetes* **54**, 1873-1878 (2005).

14. Szczerbal I, Foster HA, Bridger JM. The spatial repositioning of adipogenesis genes is correlated with their expression status in a porcine mesenchymal stem cell adipogenesis model system. *Chromosoma* **118**, 647-663 (2009).

15. Lund E*, et al.* Lamin A/C-promoter interactions specify chromatin state-dependent transcription outcomes. *Genome Res* **23**, 1580-1589 (2013).

16. Paulsen J*, et al.* Chrom3D: three-dimensional genome modeling from Hi-C and nuclear lamin-genome contacts. *Genome Biol* **18**, 21 (2017).

17. Korfali N*, et al.* The leukocyte nuclear envelope proteome varies with cell activation and contains novel transmembrane proteins that affect genome architecture. *Mol Cell Proteomics* **9**, 2571-2585 (2010).

18. Robson MI*, et al.* Tissue-Specific Gene Repositioning by Muscle Nuclear Membrane Proteins Enhances Repression of Critical Developmental Genes during Myogenesis. *Mol Cell* **62**, 834-847 (2016).

19. Zuleger N*, et al.* Specific nuclear envelope transmembrane proteins can promote the location of chromosomes to and from the nuclear periphery. *Genome Biol* **14**, R14 (2013).

20. Batrakou DG*, et al.* TMEM120A and B: Nuclear Envelope Transmembrane Proteins Important for Adipocyte Differentiation. *PLoS One* **10**, e0127712 (2015).

21. Lee YH*, et al.* Microarray profiling of isolated abdominal subcutaneous adipocytes from obese vs non-obese Pima Indians: increased expression of inflammation-related genes. *Diabetologia* **48**, 1776-1783 (2005).

22. Rosell M*, et al.* Brown and white adipose tissues: intrinsic differences in gene expression and response to cold exposure in mice. *Am J Physiol Endocrinol Metab* **306**, E945-964 (2014).

23. Haakonsson AK*, et al.* Acute genome-wide effects of rosiglitazone on PPARgamma transcriptional networks in adipocytes. *Mol Endocrinol* **27**, 1536-1549 (2013).

24. Byerly MS*, et al.* Transcriptional profiling of hypothalamus during development of adiposity in genetically selected fat and lean chickens. *Physiol Genomics* **42**, 157-167 (2010).

25. Beaulieu-Laroche L*, et al.* TACAN Is an Ion Channel Involved in Sensing Mechanical Pain. *Cell* **180**, 956-967 e917 (2020).

26. Wang ZV*, et al.* Identification and characterization of a promoter cassette conferring adipocyte-specific gene expression. *Endocrinology* **151**, 2933-2939 (2010).

27. Eguchi J*, et al.* Transcriptional control of adipose lipid handling by IRF4. *Cell Metab* **13**, 249-259 (2011).

28. Lee KY*, et al.* Lessons on conditional gene targeting in mouse adipose tissue. *Diabetes* **62**, 864-874 (2013).

29. Jeffery E*, et al.* Characterization of Cre recombinase models for the study of adipose tissue. *Adipocyte* **3**, 206-211 (2014).

30. Gonzaga-Jauregui C*, et al.* Clinical and molecular prevalence of lipodystrophy in an unascertained large clinical care cohort. *Diabetes* **69**, 249-258 (2020).

31. Worman HJ, Ostlund C, Wang Y. Diseases of the nuclear envelope. *Cold Spring Harbor Perspect Biol* **2**, a000760 (2010).

32. Mory PB*, et al.* Phenotypic diversity in patients with lipodystrophy associated with LMNA mutations. *Eur J Endocrinol* **167**, 423-431 (2012).

33. de Las Heras JI*, et al.* Tissue-specific NETs alter genome organization and regulation even in a heterologous system. *Nucleus* **8**, 81-97 (2017).

34. Wollam J*, et al.* Microbiota-Produced N-Formyl Peptide fMLF Promotes Obesity-Induced Glucose Intolerance. *Diabetes* **68**, 1415-1426 (2019).

35. Kassi E, Papavassiliou AG. A possible role of osteocalcin in the regulation of insulin secretion: human in vivo evidence? *J Endocrinol* **199**, 151-153 (2008).

36. Zhao D, Yang J, Yang L. Insights for Oxidative Stress and mTOR Signaling in Myocardial Ischemia/Reperfusion Injury under Diabetes. *Oxid Med Cell Longev* **2017**, 6437467 (2017).

37. Stanford KI, Middelbeek RJ, Goodyear LJ. Exercise Effects on White Adipose Tissue: Beiging and Metabolic Adaptations. *Diabetes* **64**, 2361-2368 (2015).

38. Pickersgill H*, et al.* Characterization of the Drosophila melanogaster genome at the nuclear lamina. *Nat Genet* **38**, 1005-1014 (2006).

39. Vogel MJ, Peric-Hupkes D, van Steensel B. Detection of in vivo protein-DNA interactions using DamID in mammalian cells. *Nat Protoc* **2**, 1467-1478 (2007).

40. Green H, Kehinde O. Sublines of mouse 3T3 cells that accumulate lipid. *Cell* **1**, 113-116 (1974).

41. Green H, Kehinde O. An established preadipose cell line and its differentiation in culture. II. Factors affecting the adipose conversion. *Cell* **5**, 19-27 (1975).

42. Peric-Hupkes D*, et al.* Molecular maps of the reorganization of genome-nuclear lamina interactions during differentiation. *Mol Cell* **38**, 603-613 (2010).

43. Wu F, Yao J. Spatial compartmentalization at the nuclear periphery characterized by genome-wide mapping. *BMC Genomics* **14**, 591 (2013).

44. Naggert JK*, et al.* Hyperproinsulinaemia in obese fat/fat mice associated with a carboxypeptidase E mutation which reduces enzyme activity. *Nat Genet* **10**, 135-142 (1995).

45. Fadason T, Schierding W, Lumley T, O'Sullivan JM. Chromatin interactions and expression quantitative trait loci reveal genetic drivers of multimorbidities. *Nat Commun* **9**, 5198 (2018).

46. Comuzzie AG*, et al.* Novel genetic loci identified for the pathophysiology of childhood obesity in the Hispanic population. *PLoS One* **7**, e51954 (2012).

47. Yang H*, et al.* Adipose-Specific Deficiency of Fumarate Hydratase in Mice Protects Against Obesity, Hepatic Steatosis, and Insulin Resistance. *Diabetes* **65**, 3396-3409 (2016).

48. Pujar MK, Vastrad B, Vastrad C. Integrative Analyses of Genes Associated with Subcutaneous Insulin Resistance. *Biomolecules* **9**, (2019).

49. Liao ZZ, Wang YD, Qi XY, Xiao XH. JAZF1, a relevant metabolic regulator in type 2 diabetes. *Diabetes Metab Res Rev* **35**, e3148 (2019).

50. Ballester M*, et al.* Integration of liver gene co-expression networks and eGWAs analyses highlighted candidate regulators implicated in lipid metabolism in pigs. *Scientific Rep* **7**, 46539 (2017).

51. Nicolaou A*, et al.* Quantitative trait locus mapping in mice identifies phospholipase Pla2g12a as novel atherosclerosis modifier. *Atherosclerosis* **265**, 197-206 (2017).

52. Pesarini JR*, et al.* Calcitriol combined with calcium chloride causes apoptosis in undifferentiated adipose tissue-derived human mesenchymal stem cells, but this effect decreases during adipogenic differentiation. *Biomed Pharmacother* **108**, 914-924 (2018).

53. Mejhert N*, et al.* Semaphorin 3C is a novel adipokine linked to extracellular matrix composition. *Diabetologia* **56**, 1792-1801 (2013).

54. Bolduc V*, et al.* Recessive mutations in the putative calcium-activated chloride channel Anoctamin 5 cause proximal LGMD2L and distal MMD3 muscular dystrophies. *Am J Hum Genet* **86**, 213-221 (2010).

55. Robson MI*, et al.* Constrained release of lamina-associated enhancers and genes from the nuclear envelope during T-cell activation facilitates their association in chromosome compartments. *Genome Res* **27**, 1126-1138 (2017).

56. Sweta S*, et al.* Importance of Long Non-coding RNAs in the Development and Disease of Skeletal Muscle and Cardiovascular Lineages. *Front Cell Dev Biol* **7**, 228 (2019).

57. Wu XM*, et al.* MicroRNA-339-3p alleviates inflammation and edema and suppresses pulmonary microvascular endothelial cell apoptosis in mice with severe acute pancreatitis-associated acute lung injury by regulating Anxa3 via the Akt/mTOR signaling pathway. *J Cell Biochem* **119**, 6704-6714 (2018).

58. Cignarelli A*, et al.* Insulin and Insulin Receptors in Adipose Tissue Development. *Int J Mol Sci* **20**, (2019).

59. Wust S*, et al.* Metabolic Maturation during Muscle Stem Cell Differentiation Is Achieved by miR-1/133a-Mediated Inhibition of the Dlk1-Dio3 Mega Gene Cluster. *Cell Metab* **27**, 1026-1039 e1026 (2018).

60. Chou CF*, et al.* KSRP ablation enhances brown fat gene program in white adipose tissue through reduced miR-150 expression. *Diabetes* **63**, 2949-2961 (2014).

61. Chen Y*, et al.* miR-155 regulates differentiation of brown and beige adipocytes via a bistable circuit. *Nat Commun* **4**, 1769 (2013).

62. Yu J*, et al.* MiR-27b-3p Inhibition Enhances Browning of Epididymal Fat in High-Fat Diet Induced Obese Mice. *Front Endocrinol (Lausanne)* **10**, 38 (2019).

63. Zhang Z*, et al.* MiR-92a regulates brown adipocytes differentiation, mitochondrial oxidative respiration, and heat generation by targeting SMAD7. *J Cell Biochem*, (2019).

64. Hou Y*, et al.* Transcriptome Analysis of Potential miRNA Involved in Adipogenic Differentiation of C2C12 Myoblasts. *Lipids* **53**, 375-386 (2018).

65. Wang L*, et al.* Obesity-Associated MiR-342-3p Promotes Adipogenesis of Mesenchymal Stem Cells by Suppressing CtBP2 and Releasing C/EBPalpha from CtBP2 Binding. *Cell Physiol Biochem* **35**, 2285-2298 (2015).

66. Xu J, Zhang L, Shu G, Wang B. microRNA-16-5p promotes 3T3-L1 adipocyte differentiation through regulating EPT1. *Biochem Biophys Res Commun* **514**, 1251-1256 (2019).

67. Delic D*, et al.* Characterization of Micro-RNA Changes during the Progression of Type 2 Diabetes in Zucker Diabetic Fatty Rats. *Int J Mol Sci* **17**, (2016).

68. Chen YQ*, et al.* Abated microRNA-195 expression protected mesangial cells from apoptosis in early diabetic renal injury in mice. *J Nephrol* **25**, 566-576 (2012).

69. Mo FF*, et al.* Jiang Tang Xiao Ke Granule Play an Anti-diabetic Role in Diabetic Mice Pancreatic Tissue by Regulating the mRNAs and MicroRNAs Associated with PI3K-Akt Signaling Pathway. *Front Pharmacol* **8**, 795 (2017).

70. Zhang L*, et al.* MicroRNA-219 decreases hippocampal long-term potentiation inhibition and hippocampal neuronal cell apoptosis in type 2 diabetes mellitus mice by suppressing the NMDAR signaling pathway. *CNS Neurosci Ther* **25**, 69-77 (2019).

71. Dooley J*, et al.* The microRNA-29 Family Dictates the Balance Between Homeostatic and Pathological Glucose Handling in Diabetes and Obesity. *Diabetes* **65**, 53-61 (2016).

72. Liu Y*, et al.* Decreased Serum microRNA-21, microRNA-25, microRNA-146a, and microRNA-181a in Autoimmune Diabetes: Potential Biomarkers for Diagnosis and Possible Involvement in Pathogenesis. *Int J Endocrinol* **2019**, 8406438 (2019).

73. Zhang XR*, et al.* Salidroside-regulated lipid metabolism with down-regulation of miR-370 in type 2 diabetic mice. *Eur J Pharmacol* **779**, 46-52 (2016).

74. Thomou T*, et al.* Adipose-derived circulating miRNAs regulate gene expression in other tissues. *Nature* **doi:10.1038/nature21365**, (2017).

75. Zheng Y*, et al.* Genome-wide association analysis of the lipid and fatty acid metabolism regulatory network in the mesocarp of oil palm (Elaeis guineensis Jacq.) based on small noncoding RNA sequencing. *Tree Physiol* **39**, 356-371 (2019).

76. El-Samahy MH*, et al.* Urinary miRNA-377 and miRNA-216a as biomarkers of nephropathy and subclinical atherosclerotic risk in pediatric patients with type 1 diabetes. *J Diabetes Complications* **32**, 185-192 (2018).

77. Carreras-Badosa G*, et al.* Altered Circulating miRNA Expression Profile in Pregestational and Gestational Obesity. *J Clin Endocrinol Metab* **100**, E1446-1456 (2015).

78. Lin ES*, et al.* Deduction of Novel Genes Potentially Involved in Keratinocytes of Type 2 Diabetes Using Next-Generation Sequencing and Bioinformatics Approaches. *J Clin Med* **8**, (2019).

79. Li H*, et al.* MiRNA-181a regulates adipogenesis by targeting tumor necrosis factor-alpha (TNF-alpha) in the porcine model. *PLoS One* **8**, e71568 (2013).

80. Ouyang D*, et al.* MiR-181a-5p regulates 3T3-L1 cell adipogenesis by targeting Smad7 and Tcf7l2. *Acta Biochim Biophys Sin (Shanghai)* **48**, 1034-1041 (2016).

81. Knarr M, Nagaraj AB, Kwiatkowski LJ, DiFeo A. miR-181a modulates circadian rhythm in immortalized bone marrow and adipose derived stromal cells and promotes differentiation through the regulation of PER3. *Scientific Rep* **9**, 307 (2019).

82. Xu Y*, et al.* microRNA-690 regulates induced pluripotent stem cells (iPSCs) differentiation into insulin-producing cells by targeting Sox9. *Stem Cell Res Ther* **10**, 59 (2019).

83. Tang X, Muniappan L, Tang G, Ozcan S. Identification of glucose-regulated miRNAs from pancreatic {beta} cells reveals a role for miR-30d in insulin transcription. *RNA* **15**, 287-293 (2009).

84. Meinke P*, et al.* A multistage sequencing strategy pinpoints novel candidate alleles for Emery-Dreifuss muscular dystrophy and supports gene misregulation as its pathomechanism. *EBioMedicine* **102587**, doi10.1016 (2019).

85. Wojtanik KM*, et al.* The role of LMNA in adipose: a novel mouse model of lipodystrophy based on the Dunnigan-type familial partial lipodystrophy mutation. *J Lipid Res* **50**, 1068-1079 (2009).

86. Kwan R*, et al.* Hepatocyte-specific deletion of mouse lamin A/C leads to male-selective steatohepatitis. *Cell Mol Gastroenterol Hepatol* **4**, 365-383 (2017).

87. Hussain I, Patni N, Garg A. Lipodystrophies, dyslipidaemias and atherosclerotic cardiovascular disease. *Pathology* **51**, 202-212 (2019).

88. Akinci B, Meral R, Oral EA. Phenotypic and Genetic Characteristics of Lipodystrophy: Pathophysiology, Metabolic Abnormalities, and Comorbidities. *Curr Diab Rep* **18**, 143 (2018).

89. Pellegrini C*, et al.* Altered adipocyte differentiation and unbalanced autophagy in type 2 Familial Partial Lipodystrophy: an in vitro and in vivo study of adipose tissue browning. *Exp Mol Med* **51**, 89 (2019).

90. Zhu Q*, et al.* Neuroendocrine Regulation of Energy Metabolism Involving Different Types of Adipose Tissues. *Int J Mol Sci* **20**, (2019).

91. Herz CT, Kiefer FW. Adipose tissue browning in mice and humans. *J Endocrinol* **241**, R97-R109 (2019).

92. Gaber EM*, et al.* Effects of a sucrose-enriched diet on the pattern of gene expression, contraction and Ca(2+) transport in Goto-Kakizaki type 2 diabetic rat heart. *Exp Physiol* **99**, 881-893 (2014).

93. Waller AP*, et al.* Sarcoplasmic reticulum Ca2+ ATPase pump is a major regulator of glucose transport in the healthy and diabetic heart. *Biochim Biophys Acta* **1852**, 873-881 (2015).

94. Guenantin AC*, et al.* Nuclear envelope-related lipodystrophies. *Semin Cell Dev Biol* **29**, 148-157 (2014).

95. Collaboration NCDRF. Worldwide trends in diabetes since 1980: a pooled analysis of 751 population-based studies with 4.4 million participants. *Lancet* **387**, 1513-1530 (2016).

96. Brown RJ*, et al.* The Diagnosis and Management of Lipodystrophy Syndromes: A Multi-Society Practice Guideline. *J Clin Endocrinol Metab* **101**, 4500-4511 (2016).

97. Sinha MK*, et al.* Analytical validation and biological evaluation of a high molecular-weight adiponectin ELISA. *Clin Chem* **53**, 2144-2151 (2007).

98. Skehan P*, et al.* New colorimetric cytotoxicity assay for anticancer-drug screening. *J Natl Cancer Inst* **82**, 1107-1112 (1990).

99. Dvinge H, Bertone P. HTqPCR: high-throughput analysis and visualization of quantitative real-time PCR data in R. *Bioinformatics* **25**, 3325-3326 (2009).

100. Smyth GK. Limma: linear models for microarray data. In: *Bioinformatics and Computational Biology Solutions Using R and Bioconductor* (ed^(eds Gentleman R, Carey V, Dudoit S, Irizarry R, Huber W). Springer (2005).

101. Raudvere U*, et al.* g:Profiler: a web server for functional enrichment analysis and conversions of gene lists (2019 update). *Nucleic Acids Res* **47**, W191-W198 (2019).

102. Jain A, Tuteja G. TissueEnrich: Tissue-specific gene enrichment analysis. *Bioinformatics* **35**, 1966-1967 (2019).

103. Benjamini Y, Hochberg Y. Controlling the false discovery rate: a practical and powerful apporach to multiple testing. *J Royal Statistical Soc Series B* **57**, 289-300 (1995).

104. Schirmer EC, Guan T, Gerace L. Involvement of the lamin rod domain in heterotypic lamin interactions important for nuclear organization. *J Cell Biol* **153**, 479-489. (2001).

105. Falcon S, Gentleman R. Using GOstats to test gene lists for GO term association. *Bioinformatics* **23**, 257-258 (2007).

Supplementary Figures

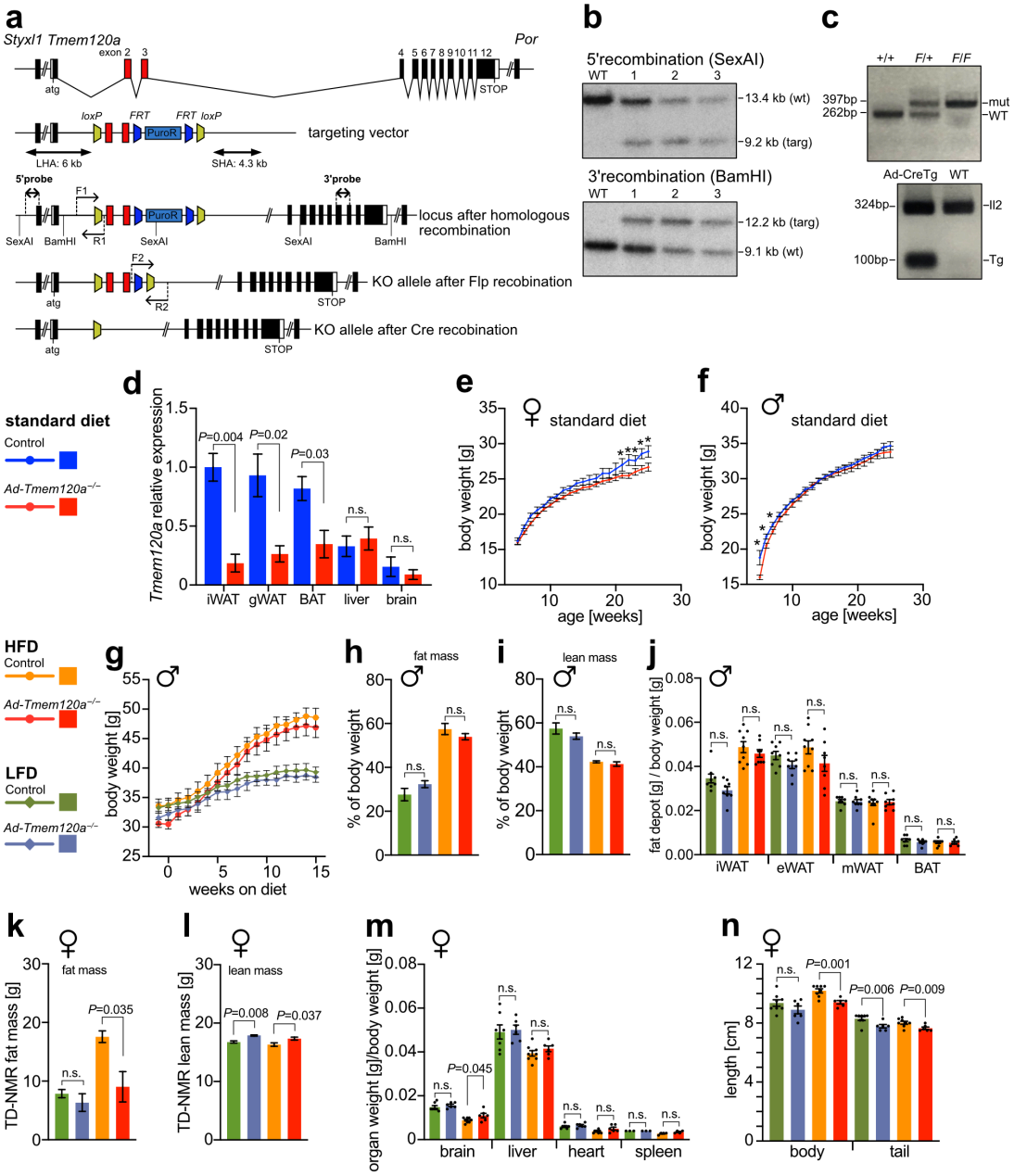

Supplementary Fig. 1, Related to Fig. 1

a-c, Strategy for adipose specific *Tmem120a*$^{-/-}$ mouse (*Ad-Tmem120a*$^{-/-}$). Exons 2 and 3 were flanked with *loxP* sites so upon expression of Cre recombinase under the adiponectin promoter *loxP* sites recombine leading to the loss of exon 2 and 3 - red boxes (**a**), the integration of targeting vector was confirmed by Southern blot with the use of 5' and 3' probes (**b**) and the animals were genotyped by PCR for the presence of the *loxP* sites and the presence of the Adiponectin *Cre* transgene – Tg (**c**). **d**, Relative expression of *Tmem120a* in subcutaneous inguinal fat by qPCR. **e** and **f**, Body weight of mice on standard diet in females, n=16-24 per genotype (**e**), and in males, n=20-25 per genotype (**f**). **g**, Males body weight on high-fat (HFD) vs low-fat (LFD) diet, shown as mean ±SEM (n=10 per genotype, per diet). **h** and **i**, Male mice body composition measured by TD-NMR after 10 weeks of LFD and HFD, fat mass (**h**) and lean mass (**i**) are shown as percent of whole-body weight; shown as mean SEM (n=5 per genotype and diet). **j**, Whole body mass-normalized weight of different adipose tissue depots in males: inguinal-subcutaneous (iWAT), epididymal (eWAT), mesenteric (mWAT) white adipose tissue and interscapular brown adipose tissue (BAT), shown as mean SEM (n=8-9 per genotype, per diet). **k** and **l**, Non-normalized female mice body composition measured by TD-NMR after 10 weeks of LFD and HFD, fat mass (**k**) and lean mass (**l**) are shown as mean mass in grams; SEM (n=4). **m**, Profile of brain, liver, heart and spleen weight, normalized to body weight in female control and knockout animals on HFD and LFD (n=6-8). **n**, Length of body nose to base of tail HFD KO shorter statistically, tail shorter both LFD and HFD in KO (n=7-8). **P* <0.05, ***P*<0.01, ****P*<0.001 by unpaired Student's *t*-test.

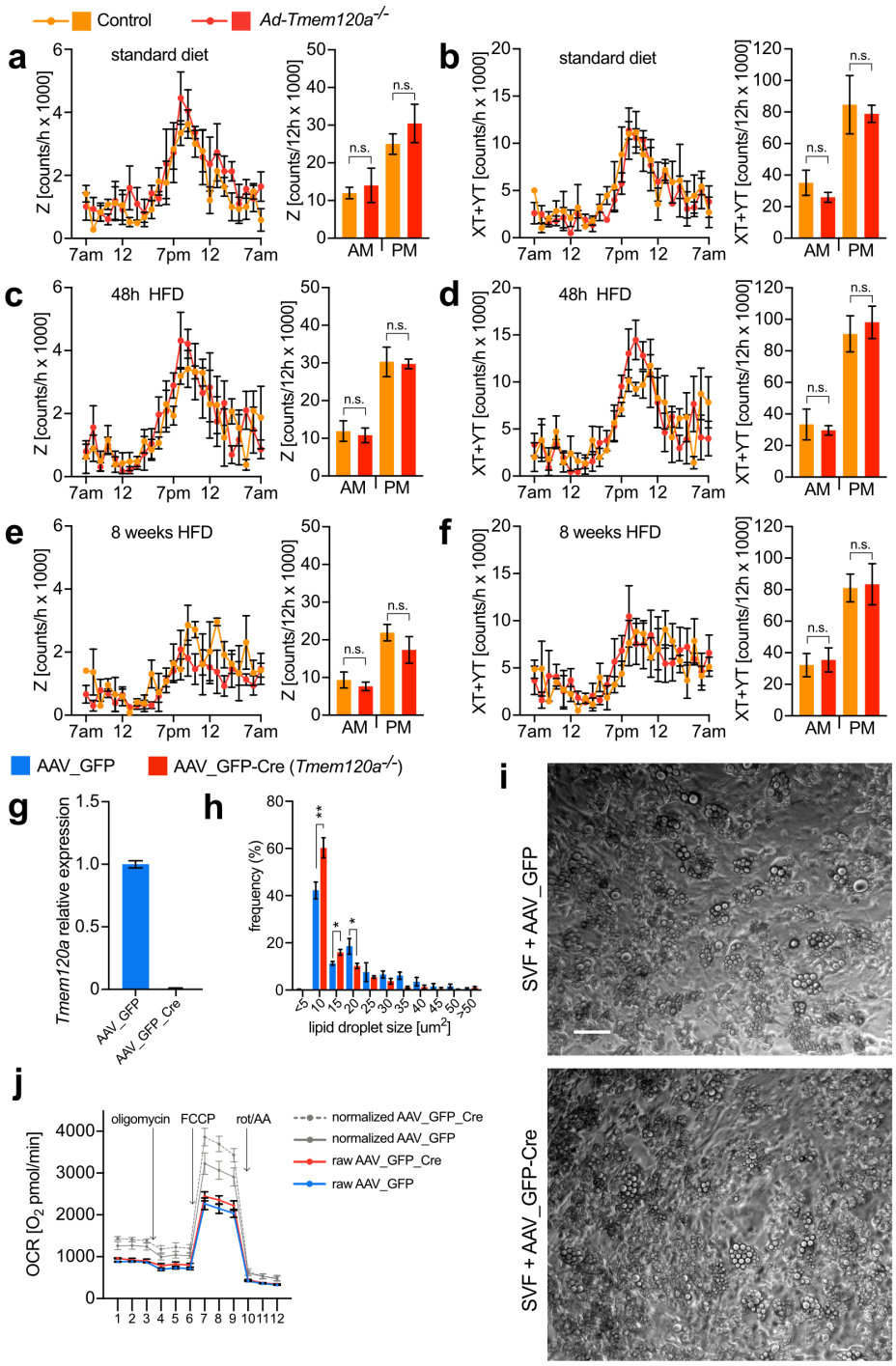

Supplementary Fig. 3, Related to Fig. 3

a and **b**, Mouse movement in indirect calorimetry chambers on standard diet. Activity data in z dimension (**a**) and activity in XY dimensions on (**b**) shown as number of infrared beams disruption during 12h cycles. Line graphs show a representative 24h trace and bar graph show the average from 48h. **c** and **d**, Mouse movement in indirect calorimetry chambers after 48h on high-fat diet. Activity data in z dimension (**c**) and activity in XY dimensions on (**d**) shown as number of infrared beams disruption during 12h cycles. Line graphs show a representative 24h trace and bar graph show the average from 48h. **e** and **f**, Mouse movement in indirect calorimetry chambers after 48h on high-fat diet. Activity data in z dimension (**e**) and activity in XY dimensions on (**f**). **g**, Expression of *Tmem120a* in differentiated SVF cells by qPCR in cells infected with AAV-GFP (Control) and AAV_GFP-Cre (*Tmem120*$^{-/-}$). **h**, Quantification of lipid droplet size in differentiated SVF cells infected AAV-GFP (Control) – blue bars and AAV_GFP-Cre (*Tmem120*$^{-/-}$) – red bars, the sizes of the lipid droplets were assigned to size bins and are shown as frequency, area in μm^2, shown as mean ±SEM, **P*<0.05, ***P*<0.01, ****P*<0.001 by unpaired Student's t test. **i**, Representative images of lipid droplets in *in vitro* differentiated SVFs, scale bars 10 μm. **j**, Comparison of total protein-normalized (grey lines) and raw (blue/red) values of oxygen consumption rates (OCR) in SVF cells differentiated into adipocytes, isolated from lox/lox animals infected with AAV_GFP_Cre and AAV_GFP. Mitochondrial stress experiment in the presence of oligomycin, FCCP, and rotenone with antimycin A (rot/AA).

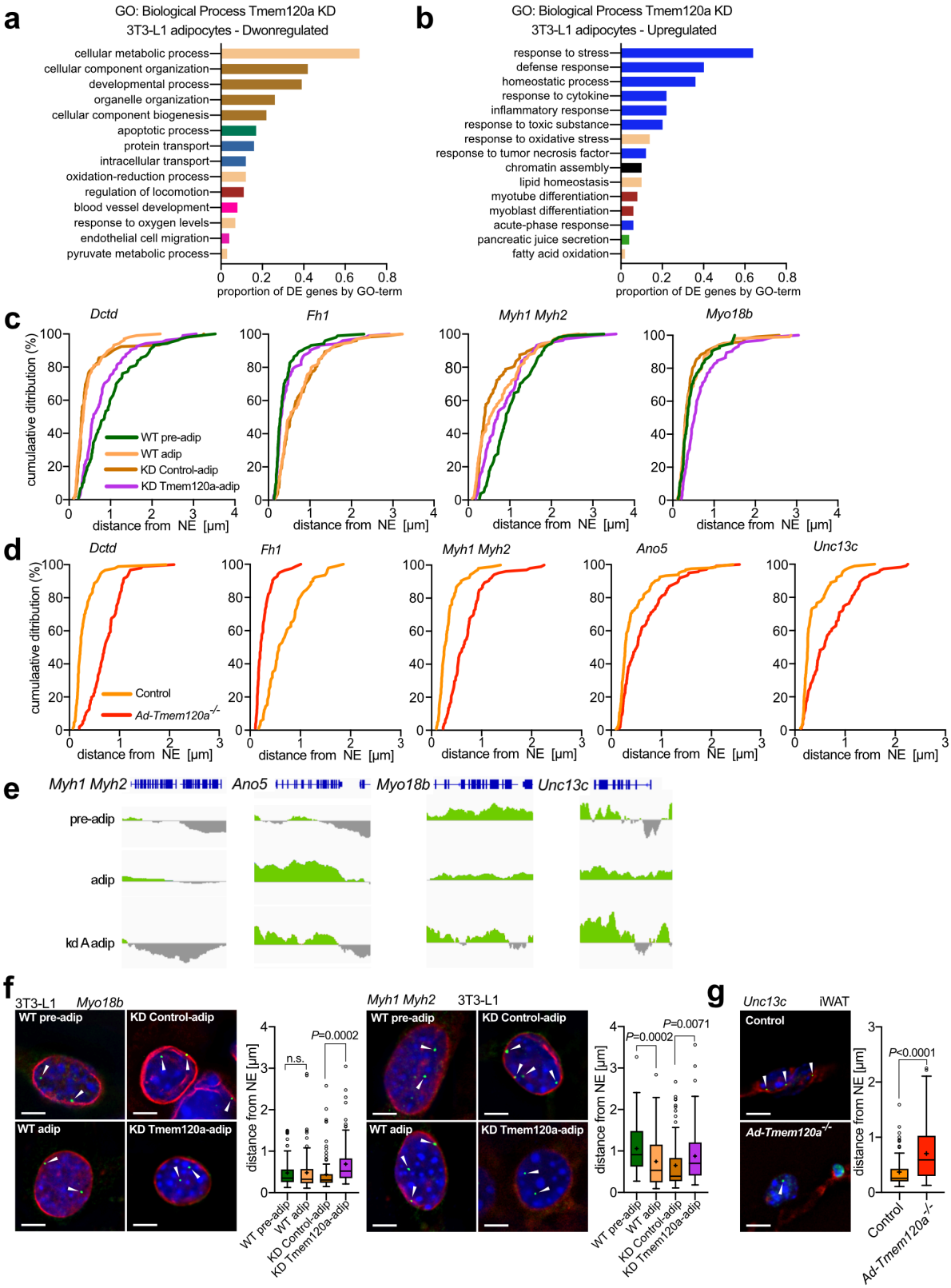

Supplementary Fig. 5, Related to Fig. 5

a and **b**, Gene ontology (GO): Biological Process of genes downregulated (**a**) and upregulated (**b**) by microarray in *Tmem120a* knockdown 3T3-L1 adipocytes. **c** and **d**, Cumulative distribution plots of gene distance from NE for data presented in main Fig. 5. Genes tested by FISH in the 3T3-L1 adipogenesis system (**c**) and FISH quantification in iWAT from control and *Ad-Tmem120a*$^{-/-}$ mice (**d**). **e**, 3T3-L1 DamID traces for additional genes tested. **f**, *Myh1/Myh2* and *Myo18b* FISH and box plot graph showing quantification of distance from NE 3T3-L1 system. **g**, *Unc13c* detection by FISH in mouse iWAT and quantification graphs. scale bars 5 µm.